UPPSALA
UNIVERSITET

Digital Comprehensive Summaries of Uppsala Dissertations from the Faculty of Science and Technology 941

Electronic and Geometric Structure of Phthalocyanines on Metals

MASUMEH-NINA SHARIATI

ACTA
UNIVERSITATIS
UPSALIENSIS
UPPSALA
2012

ISSN 1651-6214
ISBN 978-91-554-8382-1
urn:nbn:se:uu:diva-173505

Dissertation presented at Uppsala University to be publicly examined in Polhemsalen, Ångströmlaboratoriet, Lägerhyddsvägen 1, Uppsala, Friday, June 8, 2012 at 10:00 for the degree of Doctor of Philosophy. The examination will be conducted in English.

Abstract
Shariati, M.-N. 2012. Electronic and Geometric Structure of Phthalocyanines on Metals. Acta Universitatis Upsaliensis. *Digital Comprehensive Summaries of Uppsala Dissertations from the Faculty of Science and Technology* 941. 64 pp. Uppsala. ISBN 978-91-554-8382-1.

Adsorption of monolayers and multilayers of metal-free and metal phthalocyanines molecules on metal surfaces has been investigated using complementary microscopic and synchrotron-based spectroscopic techniques. It was observed by STM measurements that at monolayer coverage the adsorption direction of the metal-free phthalocyanine molecules with respect to the gold surface vary as a function of temperature, i.e. at room temperature (RT) and low temperature (LT). It was explained by the difference in strength of intermolecular and adsorbate-substrate interactions at room and low temperatures. Nature of the interaction between adsorbed species and the surfaces as a function of coverage has been further characterized by XPS measurements. Binding energy shifts as a function of coverage have been attributed to initial- and final-state effects, the latter being due to different core-hole screening for the different molecular coverage. The alignment of molecular films at both monolayer and multilayer coverages, which has been determined by XAS measurements in several cases, is also dependent upon the relative strength of molecule-molecule versus molecule-substrate interaction. Parallel alignment of the molecular film with respect to the surface is the result of significant interaction between the adsorbate and the substrate, whilst standing geometry of the molecular film is due to more significant intermolecular interactions. DFT simulations have provided further information on the nature of the adsorbate-substrate interaction as well as contribution of different molecular orbitals in XPS and XAS spectra. Moreover, investigation of alkali interaction with the phthalocyanine films revealed a significant modification in their geometric and electronic structures due to charge transfer from the alkali metal to the molecular film. However, no sign of metallization of the molecules has been observed by spectroscopic and microscopic studies.

Keywords: monolayer, multilayer, metal-free phthalocyanine, metal phthalocyanine, interaction, intermolecular, adsorbate-substrate, XPS, XAS, STM, DFT, alkali, metallization

Masumeh-Nina Shariati, Uppsala University, Department of Physics and Astronomy, Molecular and Condensed Matter Physics, 516, SE-751 20 Uppsala, Sweden.

ISSN 1651-6214
ISBN 978-91-554-8382-1
urn:nbn:se:uu:diva-173505 (http://urn.kb.se/resolve?urn=urn:nbn:se:uu:diva-173505)

To my mother

List of Papers

This thesis is based on the following papers, which are referred to in the text by their Roman numerals.

I Rubidium Doped Metal-Free Phthalocyanine Monolayer Structures on Au(111)
K. Nilson, J. Åhlund, M. -N. Shariati, E. Göthelid, P. Palmgren, J. Schiessling, S. Berner, N. Mårtensson, and C. Puglia
J. Phys. Chem. C, **114** (28), 12166 (2010)

II Photoelectron Spectroscopy Studies of Metal-Free Phthalocyanine on Au(111)
M. -N. Shariati, J. Lüder, B. Brena, I.Bidermane, S. Ahmadi, E. Göthelid, P. Palmgren, B. Sanyal, O. Eriksson, M. N. Piancastelli, and C. Puglia
In manuscript

III Charge transfer and chemical interaction of ZnPc and FePc with Au(111)
S. Ahmadi, M. -N. Shariati, S. Yu, and M. Göthelid
In manuscript

IV Valence band Photoelectron Spectra of Metal-Free and Iron Phthalocyanine: Atomic Contributions to The HOMO and HOMO-1 Features
M. -N. Shariati, B. Brena, M. de Simone, M. Coreno, C. Grazioli, and C. Puglia,
In manuscript

V Potassium-Intercalated H_2Pc Films: Alkali-Induced Electronic and Geometric Modifications
K. Nilson, J. Åhlund, M. -N. Shariati, J. Schiessling, P. Palmgren, B. Brena, E. Göthelid, F. Hennies, Y. Huismans, F. Evangelista, P. Rudolf, M. Göthelid, N. Mårtensson, and C. Puglia,
submitted to J. Chem. Phys.

Comments on my own participation:

I have made contributions to all included papers. In Paper II, I was main responsible for experimental work, data analysis and writing the experimental parts of the paper. In Paper IV, I was main responsible for experimental work for H_2Pc film, data analysis and writing the experimental parts of the paper. I have done the room temperature STM measurement of Paper I and participate in discussion. I have participated in experimental work and discussion regarding the results in paper III. In paper V, I have done some part of data analysis and contributed in writing, editing and discussion regarding to the work.

Contents

Abbreviations

Au	Gold
BE	Binding energy
DFT	Density Functional Theory
EXAFS	Extended X-ray Absorption Fine Structure
FePc	Iron Phthalocyanine
H_2Pc	Metal-free Phthalocyanine
HOMO	Highest Occupied Molecular Orbitals
OLED	Organic Light Emitting Devices
LT	Low Temperature
LUMO	Lowest Unoccupied Molecular Orbitals
MPc	Metal Phthalocyanine
NEXAFS	Near Edge X-ray Absorption Fine Structure
PES	Photoelectron Spectroscopy
Pc	Phthalocyanine
RT	Room Temperature
STM	Scanning Tunneling Microscopy
XAS	X-ray Absorption Spectroscopy
XPS	X-ray Photoelectron Spectroscopy
ZnPc	Zinc Phthalocyanine

1. Introduction

Organic molecules as low band gap materials are promising candidates for active layer in organic devices such as solar cells or organic light emitting devices (OLED)[1, 2]. Investigation of the electronic structure and transfer of charge carrier of organic molecular films through interfaces is fundamental to improve the optical and electrical properties of the molecular film based devices[3, 4, 5]. It is important to study the electronic structure of molecular films at different molecular coverage (mono and multilayer), interaction of the molecular film with the substrate as well as transfer of charge carriers in order to design and control the efficiency of molecular devices. Furthermore, modification of the electronic structure of molecular films by introducing charge dopant is crucial for charge transport in these molecular systems.

Development of new experimental instrument and techniques to investigate the physical and chemical phenomena in the molecular systems resulted a great advances in this field.

Invention of Scanning Tunneling Microscopy (STM) by Binning and Rohrer in the mid 80's was a revolution in this field[6]. It became possible to image surfaces, adsorbates and ordered molecular overlayer with resolution down to the atomic scale.

X-ray Photoelectron Spectroscopy (XPS) and X-ray Absorption Spectroscopy (XAS) are two other powerful techniques used to obtain information about occupied and unoccupied electronic states of the substrate and the molecular adsorbate, as well as the geometric orientation of the molecules on the surface. New generation synchrotron radiation facilities provide a tunable and polarized X-ray with high flux and high brilliance[7]. Combination of using a better X-ray source and high-tech devices provides more accurate and high-resolution data that give information about the physical and chemical phenomena occurring at the surfaces and interfaces of the adsorbate systems.

Phthalocyanine (Pc) molecules are macro-cyclic compounds extensively studied in recent years due to the possibility to use them in different applications. They are extensively used as pigments and dyes and as model systems for important biological system/process due to their similarity to porphyrins, hemoglobin and chlorophyll[8, 9]. Pc molecules are good candidate for application in organic solar cells or organic light emitting devices (OLED)[1, 2]. Those can also be used as the active elements in chemical sensors (gas sensors)[10, 11]

and have been successfully used in homogeneous and heterogeneous catalysis during a long period for oxidation reactions[12].

This thesis focuses on studies of correlation between molecular film properties at different thicknesses, strength of interaction of molecular film with substrate and effect of temperature on intermolecular and adsorbate-substrate interactions. Moreover, charge transport and modification of the electronic properties after alkali doping of Pc molecules have been studied.

The investigations have been carried out using complementary spectroscopic and microscopic techniques that provide detailed experimental information about the electronic and geometric structures of Pc's on substrates.

The thesis consists of eight chapters:

- Chapter 1: Introduction
- Chapter 2: Substrate and adsorbate. Includes a general introduction about the substrates, metal and metal–free phthalocyanine as the adsorbate molecule, alkali doping and types of interaction as well as growth modes.
- Chapter 3: Surface characterization techniques. This is a brief summary of the basic principle of Photoelectron Spectroscopy, X-ray Absorption Spectroscopy and Scanning Tunneling Microscopy
- Chapter 4: Equipment and experimental set-up. In this chapter, the beamline and the sample preparation are explained.
- Chapter 5: A brief research review. This chapter presents a brief review of the investigations that have been done.
- Chapter 6: Summary of results. A brief summary of the results is presented.
- Chapter 7: Summary and outlook
- Chapter 8: Populärvetenskaplig Sammanfattning

2. Substrate and molecular adsorption

Adsorption of molecules on a solid surface (e.g. a metal substrate) to form an organic thin film is affected by the chemical and physical interactions between the substrate and the adsorbate molecules. Further modification of the molecular film by introducing alkali metals into the molecular film affects its geometric and electronic properties. The substrate, the adsorbate molecule and the alkali dopant as well as their mutual interactions are discussed in the following.

2.1. Substrate

A single-crystal Au(111) substrate and a single-crystal Al(110) substrate have been used in our studies. Au is dense, soft and the most malleable and ductile known pure metal. It is a good conductor of heat and electricity. These properties make it a promising material widely used in electronic, biochemistry and physics applications[13, 14, 15]. Moreover, it is a stable material under UHV conditions and can be used for spectroscopic and microscopic investigations. Figure 2.1 shows an STM image of the $(\sqrt{3}\times 22)$ surface reconstruction of Au(111), well known as herringbone structure, consisting of alternating fcc and hcp domains separated by so-called soliton walls. Minimization of surface free energy is achieved by a zigzag structure of the soliton walls, induced by partial dislocations at the turning points, i.e, elbow sites in the structure[16].

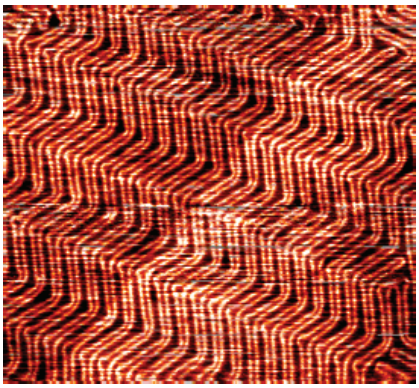

Figure 2.1: A (150 nm × 150 nm) STM image of herringbone-reconstructed Au (111) surface was taken with (-1.3V, 0.96 nA). Brighter lines are the soliton walls, forming a zig-zag structure.

Aluminum is a lightweight, soft and durable metal. It has different applications in industry and semiconductor technology. Al is used as a main conductor between components in transistors and a good contact in semiconductor devices due to its low resistivity (2.7 mohm-cm)[17, 18].

2.2. Adsorbate

Phthalocyanine molecules (Pc) are used as the adsorbed molecules in this thesis. Pc is a planar molecule, formed by four isoindole groups consisting of a pyrrole group coupled to a benzene ring. These isoindole groups are connected via nitrogen bridging (N3 in Figure 2.2) forming a macro-cyclic molecule with a void in the center. A metal atom fills the void in the center of the molecule and forms a metal phthalocyanine molecule (MPc) with four-fold symmetry. In a case of metal-free phthalocyanine molecule (H_2Pc), the hydrogen atoms are connected to two of the nitrogen atoms (N1) in the molecular center and form a two-fold symmetry molecule. Figure 2.2 shows a schematic of metal and metal-free phthalocyanine molecules.

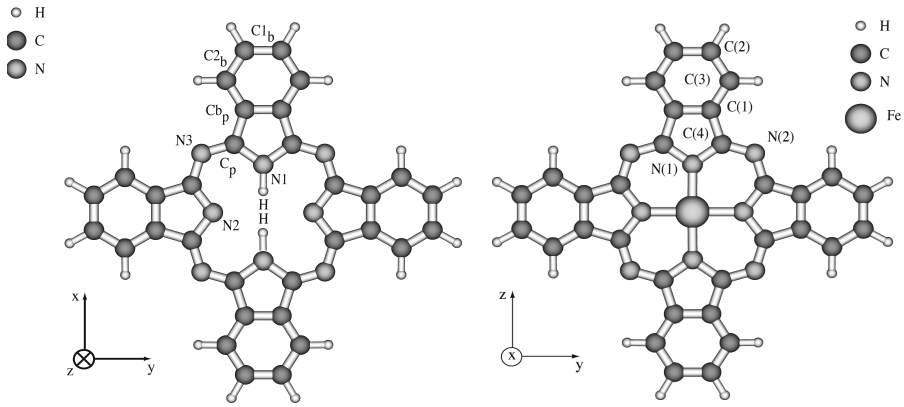

Figure 2.2: Schematic of metal and metal-free phthalocyanine. N1, N2 and N3 are three non-equivalent nitrogen atoms in the molecule and Cp and Cb correspond to the pyrrole and benzene carbon, respectively.

Phthalocyanine is used in many different applications such as solar cells, p-type organic semiconductors[19, 20], gas sensors[21], cancer therapy[22], organic light-emitting devices[23, 24] and magnetic switches[25].

The molecule is a good candidate for spectroscopic and microscopic studies due to its high thermal and chemical stability[26, 27]. Phthalocyanine thin films exist in different polymorphic forms depending on their growth conditions[28, 29].

The most common forms are called α and β phases[30, 31]. In these two phases, the molecules are arranged in columnar fashion and the molecular stacks are parallel to each other. The α and β phases are distinguished by the angle formed between the normal to the molecular plane and the stacking direction of the molecules[32]. In the case of metal-free phthalocyanine molecule, the angle is 26° and 45° in the α phase and β phase, respectively. The α phase is usually produced when the molecular film is grown onto the substrate at room temperature. Annealing of an α-phase film at a temperature about 320°C (and up to 400°C) leads to a phase transition to the β phase and forms a more compact and stable structure[25]. Moreover, another phase, called x-phase, has been reported for this molecule, that forms the angle of 42° between the normal to the molecular plane and the stacking direction[33]. This phase is considered as an intermediate phase between the α and β phases. However, the arrangement of the Pc's molecules on different substrates is under debate and the molecules do not form these phases in all cases.

2.3. Alkali dopant

Investigation of charge carriers and parameters that control the efficiency of organic molecular films is fundamental to design molecular devices. Furthermore, modification of the electronic properties of molecular films by introducing charge donation or acceptance from a dopant is crucial for charge transport in theses molecular systems [34, 35]. *p*-type molecular films are created using an acceptor-like molecule such as F_4-TCNQ that has a variety of hole transport matrices[34]. *n*-type organic molecular films are created using alkali metals[34]. Several theoretical and experimental studies of alkali doping on phthalocyanine films have been reported[36, 37, 38, 39]. Alkali doping of organic films reduces ohmic resistance of the transport layer, e.g. a molecular film, and improve the charge transport in the molecular films[34]. Moreover, an electronic phase transition from semiconductor to metallic has been reported for alkali doping of metal phthalocyanine (MPc) films[35, 37]. It has been observed that the alkali doping of MPc is a reversible process. Overdoped MPc films can be de-doped by exposing the films to oxygen that removes electrons from the film by oxidizing of the alkali metal. However recent photoemission studies of the MPc did not show metallic phase at any doping level of alkali doping [39, 40].

2.4. Types of interaction

The adsorption of atoms or molecules onto a solid substrate changes the electronic structure of the system. The adsorbates bond to the surface either via a physical interaction (physisorption) or a chemical interaction (chemisorption)[41].

Physisorption is a weak interaction, mediated via long-range van der Waals forces. Therefore, there is no significant redistribution of the electron density in the molecules and the substrate, resulting in a weak adsorbate-substrate interaction. Thus, in physisorption the electronic structure of the molecules or the atoms is not significantly perturbed upon adsorption, retaining many gas-like properties.

In contrast, chemisorption is a strong and site-specific process. The electronic structure of the adsorbate and the substrate is strongly perturbed upon adsorption, thus resulting in changes of the electron density of the system. As a result, either covalent bonds or ionic bonds are formed between the adsorbate and the substrate due to sharing of electrons. Covalent bond is usually formed between two non-metallic elements, for instance the bonds in an organic molecule, including s bonds and p bonds. Ionic bond is the chemical bond between metal and non-metal elements.

2.5. Growth modes

Epitaxial growth of thin films on a solid surface, e.g. a semiconductor or a metallic surface, is one of the important techniques in semiconductor technology. Many studies have been done in recent decades for better understanding the growth mechanism and related conditions[42, 43, 44]. A classification of the growth modes has been proposed by Bauer *et al.*[45]. They introduced three main modes, namely layer-by-layer (Frank-van der Merve, FM), island (Vollmer-Weber, VW) and layer-plus-island (Stransky-Krastanov, SK) modes. Figure 2.3 presents a schematic of the growth modes.

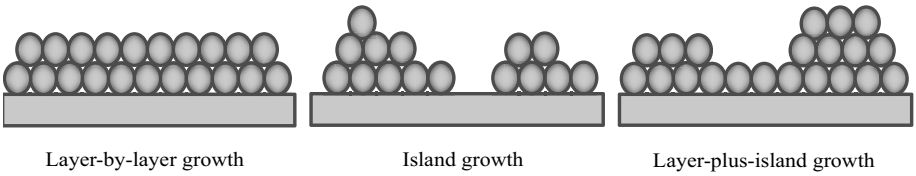

Figure 2.3: A schematic of the growth modes, namely layer-by-layer, island and layer-plus-island

The layer-by-layer growth mode is a two-dimensional growth, leading to the formation of a complete film on the substrate. In this mode, the interaction between the substrate and adatoms (adsorbate) is stronger than the interaction between the adatoms.

Instead, in the island growth mode the interactions among the adsorbates are much stronger than those between adatoms and the substrate. It leads to the formation of islands or three-dimensional adatom clusters on the substrate.

The layer-plus-island growth mode contains both the two-dimensional layer-by-layer and the three-dimensional island modes. Lattice mismatch between the substrate and the deposited film is one of the important factors that lead to this type of growth. Moreover, the surface energy of the substrate and the deposited film (overlayer) should be taken into account and determines the growth modes. If the surface energy of the substrate is higher than that of the overlayer, it will lead to either layer-by-layer or layer-plus-island growth modes. However, in the island growth mode, the surface energy of the overlayer is larger than that of the substrate.

3. Surface characterization techniques and equipment

As mentioned earlier, the invention of new experimental instruments such as Scanning Tunneling Microscopy (STM) and the development of new generation synchrotron facilities provide better tools to study the physical and the chemical phenomena occurring at surfaces and interfaces. A general description about the experimental techniques and equipment used in this thesis is presented in this chapter.

3.1. Synchrotron radiation, a unique light source

Synchrotron radiation (SR) is an electromagnetic radiation generated by charged particles, typically electrons[7]. Electrons are accelerated at almost light speed around a circular path by an electric field. The accelerated electrons emit radiation in a presence of magnetic fields that force them to travel on a curved trajectory. Synchrotron radiation is a polarized light with high flux and brilliance and the photon energy can be varied continuously from infrared (IR) (10^{-1} eV) to hard X-ray (10^{5} eV) energy range. This provides a tunable and flexible light source that makes it an ideal light source for experiments. All photoelectron spectroscopy experiments in this thesis have been performed at beamline I511 at MAX-lab, the national synchrotron radiation laboratory at Lund in Sweden. A brief introduction about the beamline is presented in the equipment section.

3.2. Concepts in spectroscopy

Spectroscopy in general is the study of interaction of electromagnetic radiation with matter. It includes a variety of techniques that provide information about physical and chemical properties of the matter. Different techniques are categorized, depending on the wavelength of the electromagnetic wave, the physical concepts and technical equipment used. For instance, X-ray Photoelectron Spectroscopy (XPS), X-ray Absorption Spectroscopy (XAS) and Ultraviolet Photoelectron Spectroscopy (UPS) are different spectroscopic techniques where photons are used in the X-ray and Ultra Violet energy

ranges (Figure 3.1). These techniques provide information about the occupied and unoccupied density of states of the studied system.

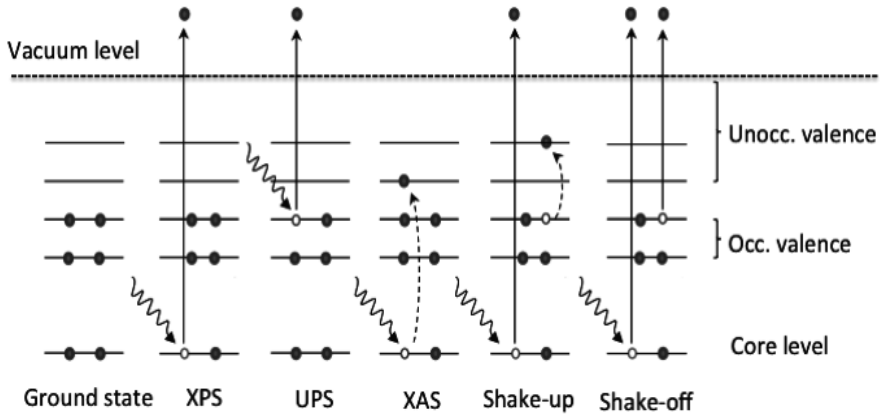

Figure 3.1: A schematic of different spectroscopic techniques

More detailed descriptions of the techniques will be presented in following sections.

3.3. Photoelectron Spectroscopy (PES)

PES is based on the photoelectric effect, described by Albert Einstein in 1905[46]. A sample is irradiated by photons and electrons are ejected from the sample if the energy of the impinging radiation is higher than the ionization potential(s). Energy conservation implies that by knowing the photon energy ($h\nu$) and measuring the kinetic energy of the photoelectrons (E_K) the binding energy (E_B) of the photoelectrons can be determined as shown in equation (3.1),

$$E_B = h\nu - E_K - \varphi \qquad (3.1)$$

E_B is the target of investigation. In the equation $h\nu$ is the known photon energy of the incoming light, E_K is the kinetic energy of the photoelectrons measured by the spectrometer, φ is the work function, i.e. energy difference between the Fermi level and the vacuum level.

The photoemission process can be divided into three steps. The first step is the photoexcitation of a core electron from a ground state with an initial energy level of E_i to a final state with energy of E_f. The photoelectron propagates in a solid (matter) in a second step and finally it escapes from the solid

surface into the vacuum level. Propagation of the photoelectron in the matter will discuss with more details further.

Intensity of PES spectrum depends on the escape depth and ionization cross section for each element. These two concepts are discussed with details further on.

Resolution of the photoelectron spectrum is limited by core-hole lifetime and resolution of the experimental devices such as spectrometer. The short lifetime of an ionized atom responds to a relatively large uncertainty in the energy of the core hole due to Heisenberg uncertainty principle. This leads to a Lorentzian broadening in the spectrum. The equipment resolution can be controlled by change of pass energy and slit width of the spectrometer. Limitation in the equipment resolution leads to a Gaussian broadening of the spectrum. Therefore, the final spectrum is a convolution of both Lorentzian and Gaussian broadening.

PES is an element-specific method, since the core-level binding energies of different elements are unique. Formation of molecules, as well as bonding between atoms and molecules with a surface, slightly changes the electron orbital energies and causes an energy shift in the spectrum. This energy shift occurs due to the presence of chemically non-equivalent atoms and is called "chemical shift". Therefore, PES is a chemically sensitive technique and is also called ESCA (Electron Spectroscopy for Chemical Analysis)[47].

X-ray photoelectron spectroscopy can be a surface-sensitive technique and can be used to study outermost atomic layers of the surface. The surface sensitivity arises from the interaction of the photoelectrons with solid (matter). The propagated photoelectrons in the solid can be elastically or inelastically scattered. In the elastic scattering, the electrons escape the solid without losing the energy and their kinetic energy is *preserved*, whereas the inelastically scatted electrons lose some of their kinetic energy on their way out from the solid.

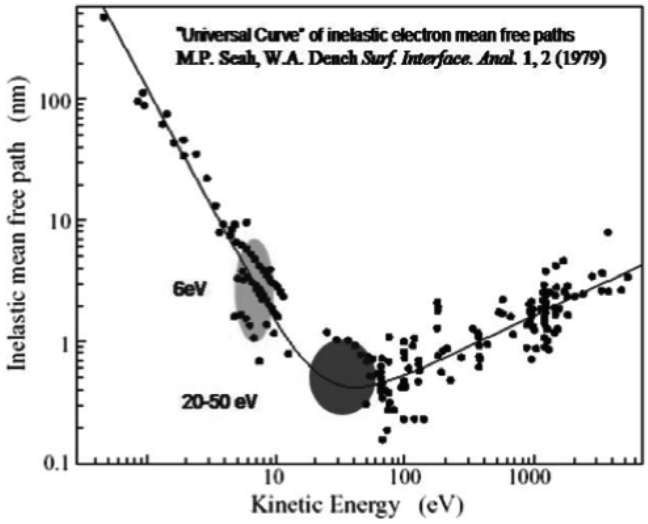

Figure 3.2: The universal curve of inelastic electron mean free path

Figure 3.2 presents the relationship between the kinetic energy and the inelastic mean free path of the electrons, the so-called "universal curve"[48]. At low kinetic energy, the electron does not have sufficient energy to interact with other electrons of the solid, resulting in a long mean free path. The low energy electron-electron scattering process occurs at the energy range between 5-20 eV, causing to excitation of plasmons in the solid. At a higher kinetic energy, the electrons on their way out from the solid can have enough energy to excite an interband transition, for instance excitation of a valence electron to a conduction band. Moreover, a photoelectron may have enough energy to ionize a core-level electron and create another photoelectron or an Auger electron. However, the electron with high kinetic energy spends less time to pass through a given thickness of solid and interact with other electrons.

At the minimum of the universal curve (20-50 eV) the mean free path is in the sub-nm range. Even at higher energy the mean free path stays well below 10 nm, making the XPS a surface sensitive technique.

3.4. Final-state relaxation in PES

Final state of PES is a photoelectron and an ionized atom or molecule. The new ionized atom or molecule will have a new potential state caused by the contraction of the system toward the nucleus. The electrons of the ionized atom or molecule are relaxed by redistribution of the electron density of the system either by rearrangement of the atomic level or charge transfers to the created core hole[49]. This process is called relaxation of the final state. The

final-state relaxation reduces the core ionization energy through these rearrangements[49, 50]. Therefore, a photoemission line in the photoelectron spectrum shifts to lower binding energy.

For an adsorbate atom or molecule onto the surface, new final-state relaxation channels will open up and surface-induced relaxation can lower the final state energy by several eV[49, 51]. This type of screening is not present for a free atom or molecule.

There are two types of screening of the adsorbate by the substrate, namely metallic screening and image potential screening[49].

The metallic screening of the adsorbate involves charge transfer from the substrate to the molecule. Strong screening of the adsorbate by the substrate is interpreted as chemisorption[52].

The image potential screening involves screening of the adsorbate on the metallic substrate. In this type of screening, the ionized state will not be screened by electron transfer from the substrate [49, 51]. Therefore, the relaxation occurs by polarization of the metallic substrate in which a charge redistribution in the metal causes a negative polarization charge. The positive charged state of the ionized atoms or the molecules is relaxed by the negative charged state of the metal substrate. These effects have been seen in both physisorption and chemisorption types of interaction of the adsorbate and the substrate[53].

Correlation of XAS and PES spectra with the final-state effect will be discussed with details in the summary part.

3.5. Satellite peaks

"Multi-electron" excitations during photoemission process lead to satellite structures namely, "shake-up" and "shake-off" peaks[50]. These peaks appear at the low kinetic energy side (higher binding energy) of the main (one-electron) photoelectron peaks. The shake-up transition is created due to excitation of a valence electron to a bound state whereas the shake-off satellite peak is created due to excitation of the valence electron to a continuum state (above the vacuum level). For instance, the shake-up transition in the C1s spectrum of metal-free phthalocyanine molecule has been studied by time-dependent density functional theory[54]. Two intensity contributions due to shake-up transitions associated to benzene and pyrrole carbons of the metal-free phthalocyanine molecule have to be taken in consideration to fit the experimental C1s photoelectron results properly.

3.6. Fermi's golden rule and ionization cross section

Fermi's golden rule (Eq. 3.2) provides information about the probability of transitions and their related intensity[55], as given in the following.

$$\omega_{fi} = \frac{2\pi}{\hbar} \left| \langle \Psi_f, K_f \left| H^{int} \right| \Psi_i, K_i \rangle \right|^2 \delta\left(E_f - E_i - h\nu\right) \qquad (3.2)$$

The transition rate depends on the strength of the coupling between the initial state and final state of the system and the density of the final state. E_i is the energy of the multi-electron system in the initial state i with the wave function Ψ_i and the wave vector K_i. E_f is the energy of the system in the final state f with the wave function Ψ_f and the wave vector K_f. The delta function $\delta\left(\mathrm{E}_f - \mathrm{E}_i - h\nu\right)$ gives condition of conservation of the energy. According to the conservation of the energy, the final state must be equal to the difference between the photon energy $(h\nu)$and the initial state energy for the function to be non-zero.

The Hamiltonian for the interaction between the electron and the photon of the electromagnetic field is determined by

$$\mathrm{H}^{int} = \frac{e}{mc} \mathrm{A} \cdot \mathrm{p} \qquad (3.3)$$

where A is the vector potential of the electromagnetic field and p is the momentum operator of the electron.

Ionization cross section is the probability of ionization from different atomic levels of an element. The Fermi's golden rule implies that the final states are different for the different spectroscopic techniques. For instance, the final states in PES can be described by the photoelectron and the remaining ionized atom or molecule. The final state in XAS is a neutral atom or molecule with an excited electron.

3.7. X-ray Absorption Spectroscopy (XAS)

XAS was first used by a theory of Kossel in the 1920s to investigate the structure of matter and was for many years referred to as "Kossel structure"[56]. XAS is a technique to probe unoccupied valence states in a presence of a core hole[57]. It is an element-specific technique due to the unique binding energy of the core electron of the different elements. The photon energy is scanned across the absorption edge to excite core electrons to unoccupied valence levels and create core holes. These core-hole states can decay (within 10^{-15} s) either by Auger electrons in low-Z elements such as N and C or by emission of fluorescence photon in high-Z elements.

The intensity of the transition is obtained from the cross section for the transition between the initial ground state and the final excited state calculated by the Fermi's golden rule (Eq. 3.4) as derived below,

$$\sigma_{XAS} \propto \left|\langle \Psi_f, \mathrm{K}_f \left| H^{int} \right| \Psi_i, \mathrm{K}_i \rangle\right|^2 \rho(\mathrm{E}_f)\delta(\mathrm{E}_f - \mathrm{E}_i - h\nu) \quad (3.4)$$

where σ_{XAS}, is the cross section of the X-ray adsorption and $\rho(\mathrm{E}_f)$ is the density of the state for the final states. This equation shows that the XA process is a "dipole interaction" between the photon and the electrons and leads to an angular dependence of the cross section. Therefore, the orientation of the molecular films or adsorbates on the surface can be probed[58]. Moreover, the "dipole selection rules" governs and transitions are allowed only if the difference of the angular momentum between the initial state and the final state is $\Delta\, l = \pm 1$. For example, in a case of a K-shell excitation, the electrons are excited from a *1s* orbital to a *p*-type orbital.

The XA spectra can be measured in three modes: Auger electron yield, partial electron yield and total electron yield. A dispersive-type electron energy spectrometer is used in the Auger electron yield by setting an energy window defined by the kinetic energy of the Auger transitions of the element of interest. In the partial electron yield, a retarding voltage is set in front of the XAS detector to retard the low kinetic energy electrons. In the total electron yield, all the emitted electrons (the photoelectrons and the Auger electrons) from the sample are detected by a multi-channel plate detector.

XAS is usually called Near Edge X-ray Absorption Fine Structure (NEXAFS) or Extended X-ray Absorption Fine Structure (EXAFS) depending on the energy range investigated. NEXAFS covers the spectral region from the threshold to about 50 eV above the edge and gives information about the unoccupied valence states of the system. EXAFS covers the region from 50 eV to several hundred eV above the edge and provide information about bond length and coordination.

This thesis concerns the NEXAFS region and the absorption spectra are recorded with the Auger electron yield mode covering a region of about 30 eV from above the edge.

3.8. Scanning Tunneling Microscopy

As mentioned earlier, the invention of the Scanning Tunneling Microscope (STM) was a revolution in the field of surface science and related areas. STM was invented by Binning and Rohrer in 1982 and they were awarded the Nobel Prize for this invention in 1986[6, 59]. This technique provides information about distribution of the electronic states at the surface and real space images of the surface with atomic resolution. Moreover, it can be used

to manipulate single atoms or molecules to form artificial structures with the atomic scale[60, 61, 62].

3.8.1. Quantum mechanical tunneling

STM is a local probe technique, which uses the concept of quantum mechanical tunneling. Indeed, electrons can tunnel through an infinite potential barrier between a very sharp metallic tip and a (semi) conducting surface, therefore creating a tunneling current[63].

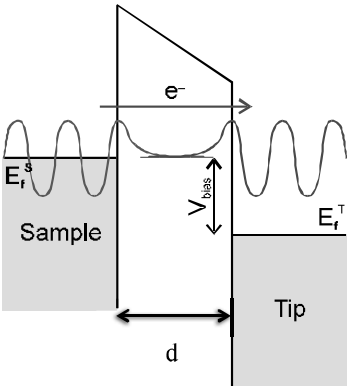

Figure 3.3: A schematic of tunneling events between a metallic tip and a metallic surface, separated by a distance *d*.

Figure 3.3 shows a schematic of tunneling events between the metallic tip and the metal surface. The tunneling probability increases exponentially with decreasing the width of the potential barrier, that is, the tip/ surface distance. Wave functions of electrons belonging to the tip and the surface can overlap when the distance between the tip and the substrate is a few Ångstrom. A bias voltage (V bias) is then applied resulting in a misalignment of the tip and surface Fermi levels, causing the electrons to tunnel from one to the other[64]. The tunneling current can be described by

$$I_t = V\rho_s(E_F^s)\exp\left(-2d\frac{\sqrt{2m\varphi}}{\hbar}\right) \qquad (3.5)$$

where d is the potential barrier width (the distance between the tip and the substrate), m is the free electron mass, φ is the potential barrier height and $\rho_s(E_F^s)$ is the density of the state of the sample at the Fermi level.

Different electronic states can be probed by changing the bias voltage[65]. In our instrument, negative bias voltage is applied to image filled states, whereas positive bias voltage are used to image empty states.

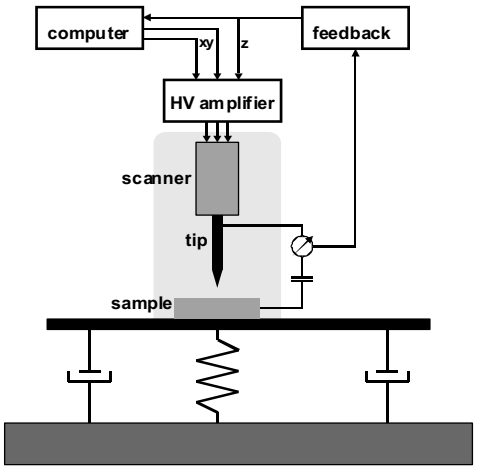

Figure 3.4: A sketch of the standard STM setup, consisting of the metallic tip, the scanner, the electronic controller and the vibration isolator[64]

3.8.2. Imaging modes

Figure 3.4 shows the important parts of a standard STM setup, consisting of a sharp metallic tip, a piezoelectric scanner, an electronic controller and a vibration isolation of the STM system. The STM tip is made by mechanically cutting or etching of thin platinum-iridium (PtIr) or tungsten (W) wires to obtain a very sharp tip, ideally with a monoatomic apex. The tips made of PtIr alloy are chemically inert and good for use in ambient condition, whereas the W tips are stiffer and good for measurement under vacuum. The piezoelectric scanner allows the tip movements with sub-Ångstrom precision. The tip scans over the substrate at a few Ångstrom (Å) distances. The electronic controller adjusts the position of the tip compared to the surface, depending on the operating conditions that are presented further. STM is a computer-based technique and all processes from providing the tunneling current, bias voltage, collecting, storing and processing of the data are done by the computer software. Moreover, a good vibration isolation of the STM system is necessary to obtain high-resolution images. In the following discussion, imaging modes of the STM system are described in details.

There are two modes of operation in STM, namely constant current and constant height modes. In the constant current mode, the tunneling current is set to a certain value typically between 0.1 nA to 10 nA. The distance between the tip and the substrate is constantly adjusted by the feedback loop during the scanning in order to keep the tunneling current constant. Therefore, the tip follows the surface structure (Figure 3.5-a). The tip-surface distance is recorded for each lateral position of the tip, i.e. $z = f(x,y)$, and gives

the topographic image of the substrate. This is the general operation mode in the STM method, although the scanning speed (rate) is limited due to finite response time of the scanner to the feedback loop.

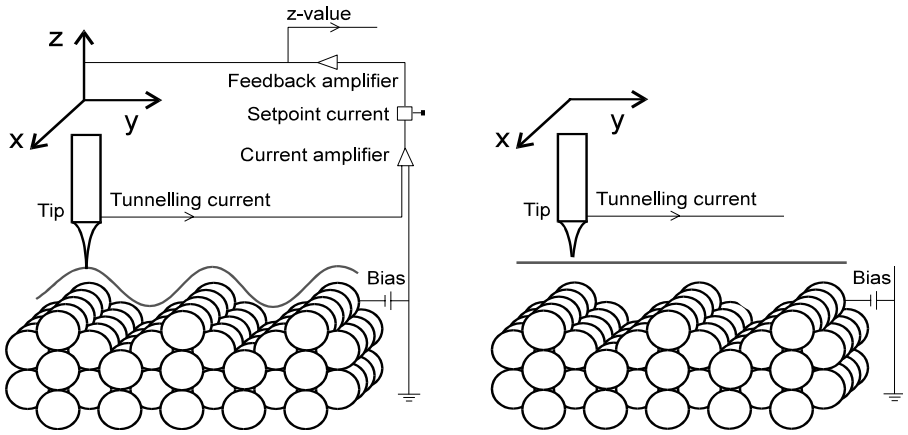

Figure 3.5: Two operation modes of the STM method. (Figure 3.5-a) The constant current mode, in which the current is kept constant by the feedback loop during the scanning. (Figure 3.5-b) The constant height mode, in which the tip scans at a constant height over the surface. (Courtesy: Emmanuelle Göthelid)

In the constant height mode, the tip scans the substrate at an absolute constant height that is chosen by the operator and the feedback loop is turned off. Therefore, the tunneling current is recorded as a function of the lateral position of the tip, i.e. I = f(x,y) (Figure 3.5-b). This operation mode has higher scanning rate due to switching off the feedback loop and is often used to observe dynamical processes[66]. However, the disadvantages of this mode are an increased risk of crashing the tip onto the substrate and a higher sensitivity to thermal drift (internal heating of the experimental equipment during normal operation) due to switching off the feedback loop. Thus, this operation mode is suitable to study atomically flat surfaces at well-controlled temperatures.

3.9. Density Functional Theory (DFT)

Density Functional Theory is a suitable method for calculation of the structure of atoms, molecules, crystals, surfaces and their interactions[67]. Theoretical simulations of the experimental results are often necessary for a correct interpretation of the spectral features. On the other hand the experimental data represent a valuable opportunity to test the validity of the description offered by different theoretical models of spectroscopic results[68].

Part of the presented results in this thesis was obtained within an experiment-theory collaboration. We compared our measurements with Density Functional Theory (DFT) simulations of the x-ray spectra. We could thus exploit the combination of experiment and theory to determine the contributions of different molecular orbitals in the valence spectra as well as the mechanisms of adsorbate-substrate interactions. DFT calculations have provided accurate and valuable interpretations of the experimental results in the papers II, IV and V. Different simulation methods and assumptions have been explained in the theoretical method part of the above articles.

4. Equipment and experimental set-up

The experimental set-up, including equipment as well as sample preparation, will be explained in this chapter. All photoelectron spectroscopy experiments have been performed at the surface end station of beamline I511 at MAX-Laboratory in Lund, Sweden. This beamline has been equipped with different devices in order to have better control of sample preparation and high accuracy in the experimental performance. The following part is a short description of this beamline.

4.1. Beamline I511, MAX-lab

The photoelectron spectroscopy and X-ray absorption experiments were performed at beamline I511 at MAX-Lab. This is an undulator-based beam line[69]. The surface end station of the beamline consists of two chambers, an analysis chamber and a preparation chamber with base pressures of 8×10^{-11} and 5×10^{-10} mbar, respectively. The analysis chamber is equipped with a Scienta R4000 hemispherical electron analyzer, which can be rotated around the photon beam axis. Due to the end-station construction the incoming light is always hitting the sample at a grazing angle of 7° off the surface plane. The preparation chamber is equipped with sputtering and annealing facilities, LEED, mass spectrometer and evaporators. The sample holder (manipulator head) can be rotated independently, making it possible to change the angle between the surface and the E vector of the incoming light.

The XAS spectra were detected at two different geometries with the electric field vector E of the light parallel and perpendicular to the surface.

Figure 4.1 is a sketch of a typical hemispherical analyzer. It consists of several parts, mainly electrodes for acceleration, collection and focusing of the emitted electrons from the sample into the hemispherical part. The hemispherical part consists of two inner and outer electrodes. Electrons with different kinetic energy pass through the hemispherical part, but only the electrons with kinetic energy equal to the pass energy (E_P) can be imaged in the middle of detector. These electrons pass through the hemispherical analyzer with a curve trajectory with the mean radius of $\bar{R}=(R_{in} + R_{out})/2$.

Energy resolution (ΔE) of the spectrum is obtained by the following equation.

$$\Delta E = E_P \times S/2.\bar{R} \qquad (4.1)$$

where S is the entrance slit and $\bar{R}$ is the mean radius of the analyzer.

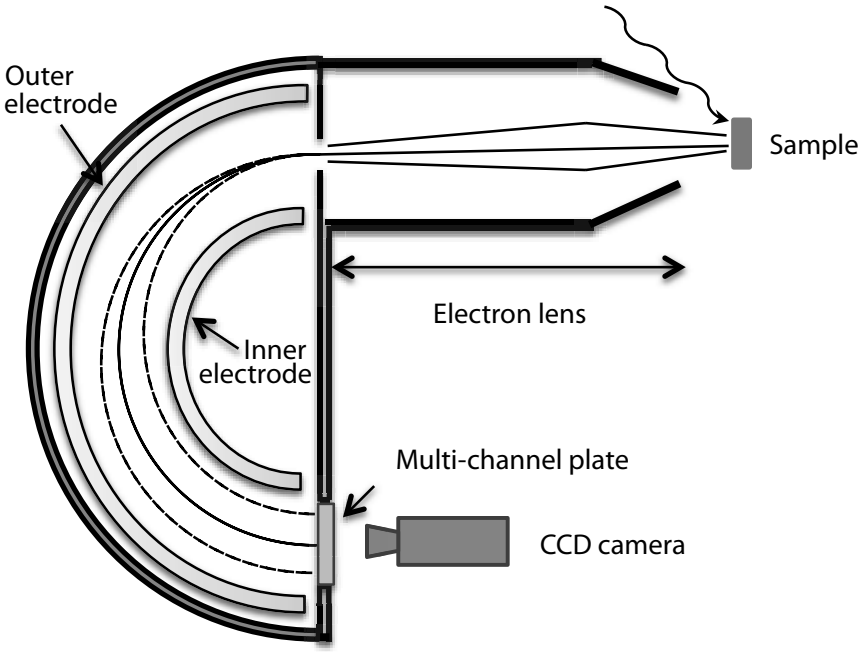

Figure 4.1: A sketch of a typical hemispherical analyzer, consisting of different electrode parts, hemispherical part, multi channel plates (MPC) and CCD camera.

4.2. Sample preparation

The single-crystal Au (111) substrate was purchased from Surface Preparation Laboratory-SPL Company. The $\left(\sqrt{3} \times 22\right)$ surface reconstruction of Au (111) was prepared by cycles of argon sputtering and annealing to 720 K. The H_2Pc molecule was purchased from Aldrich (98% dye content). The molecules were deposited, in situ, onto the sample in an evaporation chamber under UHV conditions, using a home-built evaporator positioned a few centimeters away from the substrate. The evaporator consisted of a quartz glass tube with a diameter of about 5mm with a tungsten heating wire twisted around it. The evaporator and the molecules were outgassed carefully before the deposition. The evaporation temperature was controlled by careful adjustment of the current used to heat the glass tube. The sample was kept at room temperature during the deposition of the molecules. The monolayer was prepared by annealing of the multilayer at 670 K.

5. A brief research review

Phthalocyanines (Pcs) have been studied extensively in the last two decades. A brief review of studies about geometric and electronic structure of phthalocyanines at different molecular coverages and modification of the molecular film after alkali metals intercalation is presented in this chapter.

5.1. Phthalocyanine monolayer and multilayer films on different substrates

Studies of adsorption behavior, electronic structure and transfer of charge carrier of organic molecular films at different molecular coverages are fundamental to improve the optical and electrical properties of the molecular film based devices[3, 4, 5]. STM studies of metal phthalocyanines such as FePc, CuPc and CoPc on Au(111) substrate have revealed that the molecules at monolayer coverage are aligned with their molecular plane parallel to the surface forming a highly-ordered adlayer with a square unit cell. The molecules in the multilayer film (from the second and third layers to higher thicknesses) are standing on the surface, i.e. with the molecular plane tilted with respect to the surface normal[70, 71, 72]. Furthermore, standing geometry or tilting of the molecular plane in the multilayer films have been confirmed by XAS studies of multilayer films of H_2Pc on conductive glass (FTO)[26] and graphite[73] and FePc on Si(100)[74]. For such systems, the standing orientation of the molecular plane has been interpreted as a sign of a more significant molecule-molecule interaction with respect to the monolayer case, where the molecule-substrate interaction would has an important role.

Moreover, PES studies of the phthalocyanine overlayers at different molecular covereges, i.e. monolayer and multilayer film, provide information about the electronic structure of the molecular film and the strength of interaction between the adsorbate and the substrate. Weak van der Waals forces have been reported upon investigations of adsorption of H_2Pc and ZnPc on InSb(001), since the spectral appearance of the monolayer and the multilayer spectra did not change drastically[75, 76]. However, studies of a H_2Pc molecular film on TiO_2(110) showed that the C1s core-level spectrum of the monolayer is strongly modified [77]. It was found that the reactivity of the substrate signif-

icantly affects the strength of the adsorbate-substrate interaction. The bridging oxygen atoms on the TiO_2 and dangling bonds of the Si substrate are known to make such surfaces reactive causing chemical interactions between the adsorbate and the substrate[77, 78].

5.2. Alkali-doped phthalocyanine films

Modification of the electronic structure of organic molecular films by introducing alkali dopant is an object of interest recently. STM studies and transport measurement of alkali doped metal phthalocyanine (MPc) films revealed an electronic phase transition from semiconductor to metallic phase[35, 37]. It has been observed that the alkali doping of MPc is a reversible process. Over-doped metal phthalocyanine films can be de-doped by exposing the films to oxygen that removes electrons from the film by oxidizing the alkali metal. Theoretical studies of K-doped ZnPc and MgPc have predicted an observation of an insulator-to-metal transition of Pc films upon alkali intercalation[79]. Moreover, room-temperature conductance measurements of MPc molecules as a function of K concentration (between 0 and 4 K atoms per molecule) have revealed that the electronic structure of the molecular film changes drastically by alkali doping from insulator–to-metal depending of doping level, as reported in a work by Cracium et al.[37]. However, these results have not been confirmed by any other subsequent study. Recent valence band photoemission studies of the MPc such as CoPc, FePc and CuPc did not show metallic phases at any alkali doping level[39, 40].

6. Summary of results

A brief summary of the results is presented in this chapter. The results in the first section concern molecular film properties at different thickness, strength of interaction of the molecular film with the substrate and effect of temperature on intermolecular and adsorbate-substrate interactions. Furthermore, modification of the geometric and electronic structures after alkali doping of Pc molecules is discussed in the second section of this chapter.

6.1. Adsorption of metal and metal-free phthalocyanine on Au(111) at different molecular thicknesses

It is fundamental to investigate electronic structure of molecular films at different molecular coverages (mono and multilayer), interaction of the molecular film with the substrate as well as charge transfer processes in order to design and control the efficiency of molecular devices. In the following, our results will be presented, which cover these fundamental subjects.

6.1.1. Temperature-dependent adsorption of H_2Pc monolayers on Au(111) (paper I)

Adsorption of monolayers of metal-free phthalocyanine molecules (H_2Pc) on the Au(111) $\left(\sqrt{3} \times 22\right)$ reconstructed surface has been investigated by Scanning Tunneling Microscopy (STM) at room temperature (RT) and low temperature (LT), namely 70 K. STM images of the system at both temperatures revealed that the monolayer forms a densely-packed structure on the substrate with a square unit cell, and the molecules are aligned with their molecular planes parallel to the surface (Figure 6.1). Table 6.1 lists the values for the lattice parameters of H_2Pc adsorbed on the Au(111) surface. It was found that the angle between molecular adsorption direction and the $\langle 11\bar{2} \rangle$ crystallographic orientation of the substrate is significantly changed from 30° at LT to ± 60° at RT.

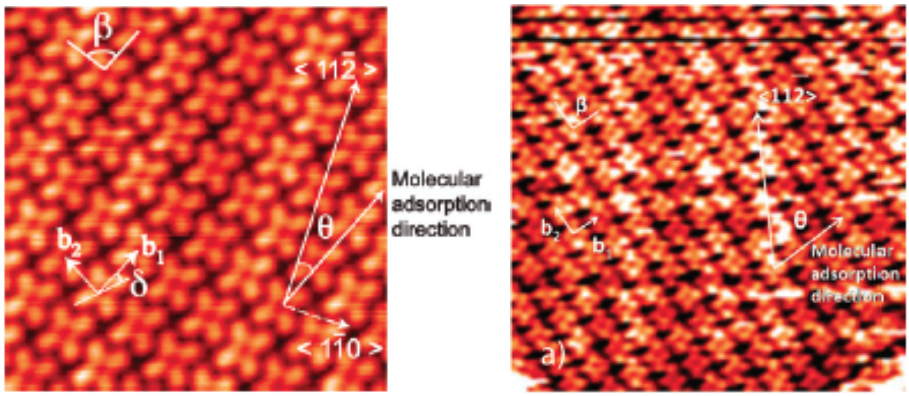

Figure 6.1: Low-temperature (left image, -1.45 V, 0.17 nA, 10.4 nm x 10.4 nm) and room-temperature (right image, -1.74 V, 1.01 nA, 21 nm x 18.6 nm) STM images of the monolayer coverage of H_2Pc on the Au (111). b1 and b2 represent the unit vectors, β is the angle between the unit vectors and θ is the angle between the molecular adsorption direction and the crystallographic direction of the substrate

This difference is due to the adsorption behavior of the molecules onto the substrate at different temperatures. The difference becomes more evident in larger-scale images. Figure 6.2 shows the adsorption of H_2Pc on the herring-bone reconstructed Au(111) surface at LT (left image) and RT (right image).

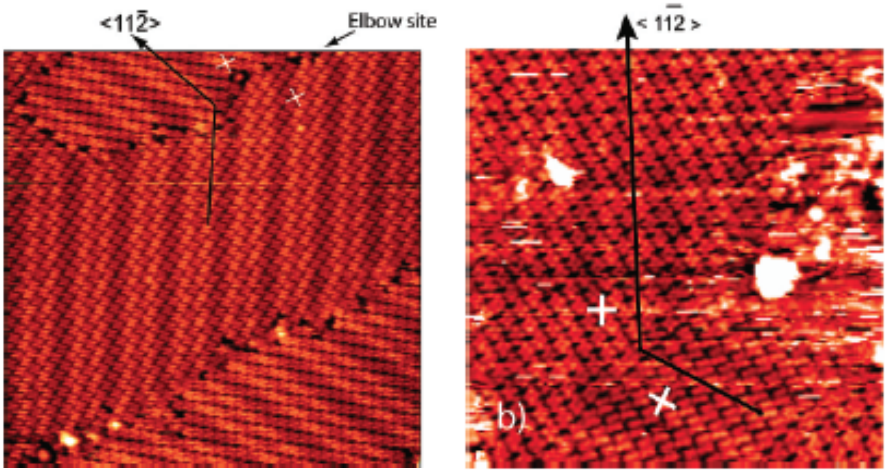

Figure 6.2: Low-temperature (left image, -1.75 V, 0.03 nA, 54.8 nm × 54.8 nm) and room-temperature (right image, -1.74 V, 1.01 nA, 35.6 nm × 33.6 nm) STM images of the monolayer coverage of H2Pc on the Au (111). Crosses in the images indicate the symmetry axes of the molecules from one domain to the other.

The molecular adsorbates on the surface reconstruction are clearly visible in the STM images. The bright rows correspond to the soliton walls of the gold

herringbone reconstruction following the $\langle 11\bar{2} \rangle$ direction of the substrate. At LT, the H_2Pc molecules form domains with well-defined boundaries, following the elbow sites of the gold herringbone reconstruction. It can be seen in the corresponding images that the adsorption direction of the molecules is dependent on the underlying reconstruction and follows the substrate structure, i.e. the molecular adsorption direction changes at the elbow sites. However, the orientation of the molecular symmetry axes (x and y) stays identical from one domain to the other, as evidenced by the two crosses in the image.

In contrast, RT STM studies of the system (right image in Fig. 6.2) showed that the angle between the molecular adsorption direction and the substrate $\langle 11\bar{2} \rangle$ direction varies, with an angle of about ± 60°. Indeed, the adsorption direction of the molecules remains unchanged across the elbow sites, the molecules themselves rotating instead to follow the underlying substrate structure. The symmetry axes (x and y) of the molecules at the elbow site are shown with crosses in the image. Therefore, very few domain boundaries are created in this temperature. These results are similar to what has been found in LT STM studies of FePc adsorption on Au(111)[70, 80]. It was reported that at monolayer coverage the adsorbate molecules rotate at the elbow site to follow the substrate structure.

These differences observed for the molecular adsorption at the two studied temperatures can be explained by the strength of molecule-molecule and molecule-substrate interactions. At LT, the intermolecular interaction is more significant, keeping the orientation of the molecules themselves constant from one domain to the other, thus causing a change in the molecular adsorption direction at the elbow sites. At RT instead, STM studies of H_2Pc on Au indicate that adsorbate-substrate interaction plays an important role, resulting in rotation of the molecule at the elbow sites, allowing their adsorption direction to remain unchanged. The same argument is valid in LT STM studies of adsorption of FePc on Au (111), where molecule-substrate interaction was more significant in the monolayer coverage, causing the rotation of the molecules at the elbow site.

Unit cell	H_2Pc LT	H_2Pc RT
b_1	1.43 ± 0.04 nm	1.51 ± 0.08 nm
b_2	1.38 ± 0.07 nm	1.44 ± 0.03 nm
β	87.7° ± 1.0°	~90°
θ	29.7° ± 1.5°	± 60°
δ	27.4° ± 1.9°	varying

Table 6.1: Values for the parameters of H_2Pc adsorbed on Au(111) at low and room temperatures

6.1.2 Geometric and electronic structure of H_2Pc monolayer and multilayer film on Au(111) (paper II)

Adsorption of monolayers and multilayers of metal-free phthalocyanine molecules (H_2Pc) on Au(111) $\left(\sqrt{3} \times 22\right)$ reconstructed surface (at room temperature) was investigated by X-ray Photoelectron Spectroscopy (XPS) and X-ray Absorption Spectroscopy (XAS).

The carbon 1s core-level photoemission (PE) spectrum for the monolayer exhibits a two-component spectral feature while the multilayer spectrum consists of three main features (Figure 6.3.a). In both the monolayer and the multilayer spectra, the most intense peak at lower binding energy (284.1 eV and 284.9 eV respectively) corresponds to benzene-type carbon atoms. The second peak, at 281.3 and 286.5 eV for the monolayer and multilayer respectively, is due to pyrrole-type carbon atoms together with the shake-up transitions associated with the benzene carbons. Finally, a low-intensity peak at 288.4 eV BE is resolved in the multilayer spectrum, and is associated with the shake-up transition of almost exclusively pyrrole carbons.

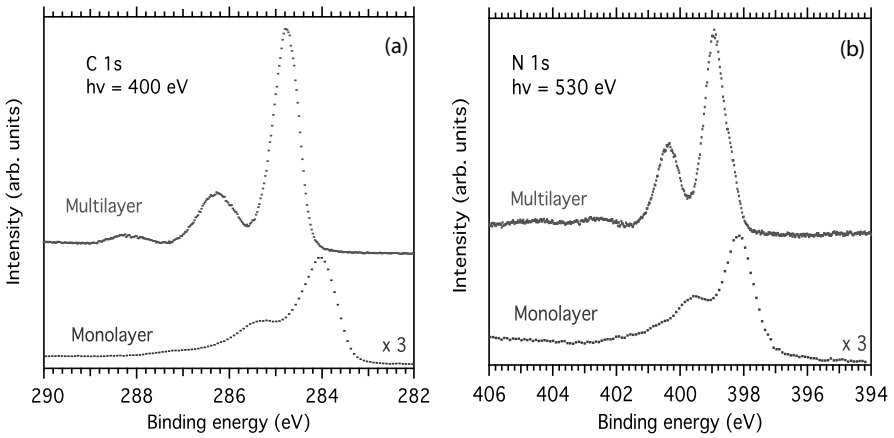

Figure 6.3: C1s and N1s PE spectra of the monolayer and the multilayer coverages of H_2Pc on Au(111)

Figure 6.3.b presents N1s core-level spectra obtained on the phthalocyanine monolayer and multilayer. The monolayer spectrum exhibits a main peak at 398.1 eV followed by a (low intensity) feature at 399.6 eV. The multilayer spectrum consists of two main components at 398.9 and 400.4 eV BE, followed with two broad intensity features at 402.6 eV and 404.6 eV BE. These components (and features) are associated to the three non-equivalent nitrogen atoms in the molecule and the shake-up and shake-off transitions, respectively.

Comparison of the binding energy of the different components in the monolayer and the multilayer spectra of C1s and N1s shows a shift to higher

BE for the multilayer with respect to the monolayer. This can be attributed to final-state effects, i.e. different core-hole screening for the different molecular coverage. Moreover, in the monolayer film, the interaction between the molecular overlayer and the substrate is stronger than in the case of the multilayer film as m. As a result, the electronic structure of the molecular film is perturbed by the substrate, causing a redistribution of the electron density of the system, manifested by the changes of the spectral appearance of the monolayer spectrum in comparison with the multilayer spectrum, the later being more similar to the molecular (gas phase) spectrum[54]. Thus, the binding energy shift and the small changes of the line appearance observed in the spectra of the mono- and the multilayer can be also related to initial-state effects, i.e to the different interaction between the adsorbate and the substrate for the two coverages. The broadening and the binding energy separation of the two main peaks in the C1s XP spectra (1.2 eV for multilayer and 1.6 eV for monolayer) can be regarded as a fingerprint of surface-induced modification of the molecular layer.

This is further confirmed by X-ray Absorption Spectroscopy (XAS) studies, which show a decreased density of unoccupied states due to charge transfer from the Au substrate to the molecules. N1s XAS measurements were performed on the monolayer and multilayer film with the polarization E vector of incoming light aligned perpendicular ($E_{\perp}$, right spectra in Figure 6.4) and parallel to the surface ($E_{\parallel}$, left spectra in Figure 6.4).

At E⊥, the monolayer spectrum shows a π^* feature at 398.3 eV together with very low-intensity peaks at 399.9 eV and 401.9 eV. For the multilayer film, a high-intensity π^* feature is observed at 398.2 eV, together with lower intensity peaks at 399.9 eV and 402.3 eV, followed by a low-intensity σ^* feature at 403.6 eV. A previous theoretical study on a single H_2Pc molecule based on Density Functional Theory (DFT) calculations revealed the atomic origin of the N K edge absorption peaks[26].

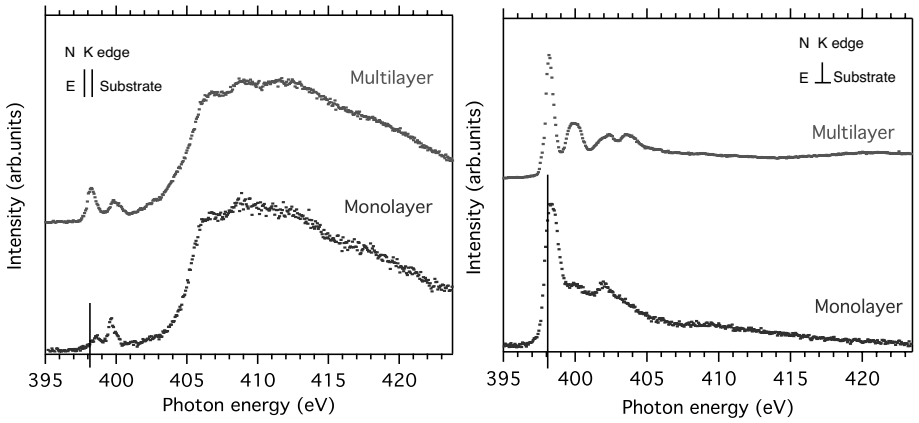

Figure 6.4: N1s XAS spectra of monolayer and multilayer films of H_2Pc/Au (111) at two different experimental geometries: (right panel) where the E vector of the incoming light is perpendicular and (left panel) parallel to the surface. Solid black lines in the XA spectrum of the monolayer (for both experimental geometries) mark the N1s PE binding energy of the monolayer

The relative intensities of the π^* and σ^* features for the two experimental geometries reveal that the molecules both in the monolayer and in the multilayer films are aligned with the molecular plane parallel to the surface. We had already found such a parallel orientation of the H_2Pc in the monolayer on Au(111) in our previous STM study (paper I) where we could observe that the monolayer forms a densely-packed structure on the substrate with a square unit cell. However, concerning the multilayer coverage, the parallel alignment of the molecules with respect to the surface is in contrast with what has been reported for other multilayer systems such as H_2Pc on conductive glass (FTO)[26] and graphite[73] and FePc on Si(100)[74] where the molecules had been oriented in standing geometry with respect to the surface.

In our investigated system, the influence of the Au substrate seems to be strong enough to cause the monolayer affects the orientation of the subsequently deposited molecular layers within the film.

Our results indicate that the interaction of the molecule with the surface affects the N1s XA spectrum for the monolayer. Observation of changes in the intensity of the LUMO (Lowest Unoccupied Molecular Orbitals) peaks of the monolayer compared with the one for the multilayer XA spectrum supports this argument.

The intensity in XAS is related to the occupancy of the orbital that the core electron is excited into. Then the different intensity of such threshold peaks (LUMO peaks) can be related to a charge transfer from the substrate to the molecules, indicating a quite significant molecule-surface interaction.

Furthermore, the interaction between H_2Pc and the Au substrate has been analyzed by DFT calculations. A side view image of Figure 6.5 shows of the relaxed molecule (slightly bucking of 0.3 Å) with an average distance of 2.9 Å from the surface. Within the molecule, the central N bound to H has the largest distance to the surface, 3.1 Å, while the benzene rings are closer to the surface with a distance of 2.8 Å. One of the molecular symmetry axes is aligned parallel to a surface lattice vector, in agreement with the STM measurements on the same system performed by our group[27].

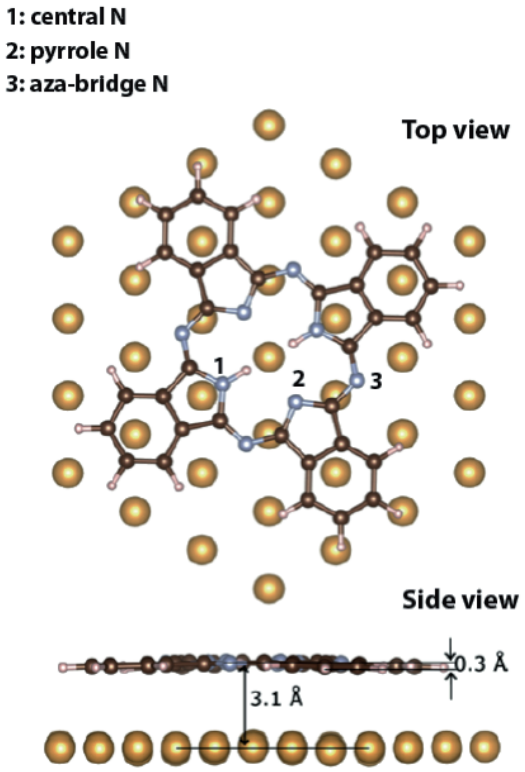

Figure 6.5: Hexagonal gold cluster consisting of 37 gold atoms of the Au(111) substrate top layer, plus the relaxed adsorbed H_2Pc. One of the molecular symmetry axes is aligned parallel to one surface lattice vector. The molecule shows an overall vertical distortion of 0.3 Å due to interaction with the surface. Yellow spheres: gold atoms; brown spheres: carbon atoms; light blue spheres: nitrogen atoms; white spheres: hydrogen atoms.

Monolayer XAS simulated spectra at the experimental geometries with the E vector almost parallel and perpendicular (7° and 83°) to the substrate are shown in figure 6. 6 and 6. 7. In the geometry of E parallel (7°), the first small peak is partly due to the 7˚ tilted experimental configuration, which results in a projection of π states onto the measurement. In the inset of this

figure, we have compared the threshold region of the XA spectrum of the relaxed molecule with and without the gold cluster. Therefore, the features at lower energies (between 397 and 398 eV) arise from the interaction with the gold atoms. These peaks are generated by pyrrole and aza-bridge N atoms. The second peak has small contributions deriving from the molecular distortion induced by the adsorption, as can be seen in the total XAS of the single molecule at 0° in Figure 6.6. However, larger contributions arise from interactions with the surface.

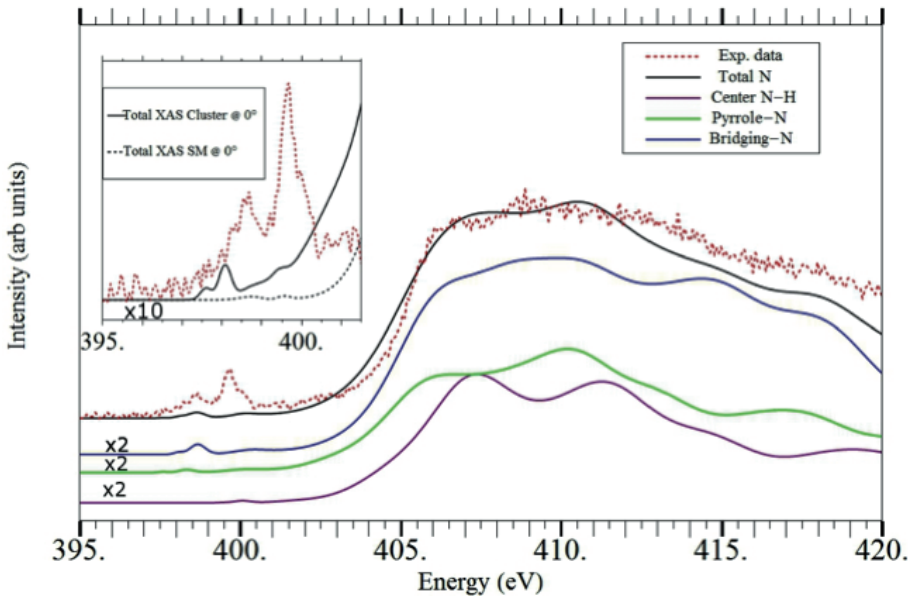

Figure 6.6: Experimental (red dotted line) and total theoretical (black line) N1s XA spectra for the $E_{\parallel}$ configuration. The calculated spectrum is simulated for an angle of 7° between the molecular plane and the E vector. The contributions of all the different N species e.g. center N-H (purple line), pyrrole-N (green line) and aza-bridge-N (blue line) are plotted. In the inset we show the photon energy region between 395.0 to 401.5 eV. The black line is the total theoretical curve XAS at 0° between the molecular plane and the E vector, and the black dashed curve is the single-molecule calculation at 0°.

Figure 6.7 shows the XA simulation at the geometry with the E vector perpendicular to the surface (83°). The first peak at 398.5 eV is originated by the pyrrole and by the aza-bridge N. A comparison with the single-molecule calculations (not presented here) shows that the shoulder at lower energy (about 397.5 eV) arises from the interaction with the gold cluster. The second peak (at about 400 eV), which has lower intensity compared to the multilayer case, has contributions from all nitrogen species.

The XAS results indicate a combination of charge transfer and molecular structure deformation upon adsorption on the Au(111) substrate.

Since the line profiles in the C1s and N1s XP spectra of the monolayer are not so drastically changed with respect to the multilayer (more molecular-like case) we cannot exclude that what we see in the XAS spectra could be due to some strong interaction channel, which opens as the core hole is created[81].

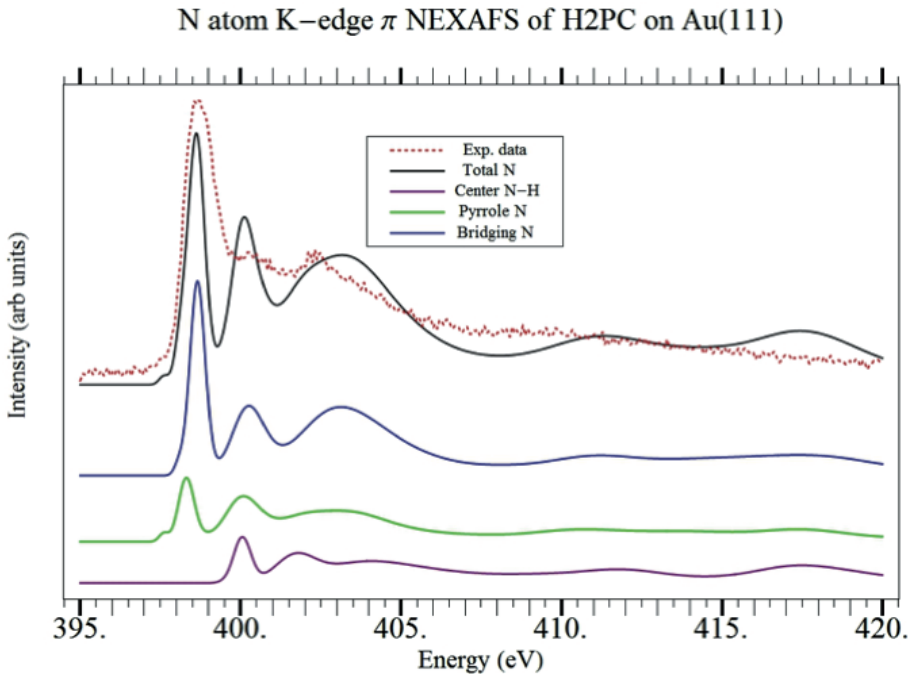

Figure 6.7: Experimental (red dotted line) and total theoretical (black line) N1s XA spectra for the E⊥ configuration. The calculated spectrum is simulated for an angle of 83° between the molecular plane and the E vector. The contributions of all the different N species e.g. center N-H (purple line), pyrrole-N (green line) and aza-bridge-N (blue line) are plotted.

6.1.3 Geometric and electronic structure of MPc monolayer and multilayer film on Au(111) (paper III)

Adsorption of monolayers and multilayers of zinc phthalocyanine (ZnPc) and iron phthalocyanine (FePc) molecules on Au(111) $\left(\sqrt{3} \times 22\right)$ reconstructed surface has been investigated by X-ray Photoelectron Spectroscopy (XPS) and X-ray Absorption Spectroscopy (XAS).

Figure 6.8 (left panel) shows the carbon 1s core-level photoemission (PE) spectra for the monolayer (ML) and thick films (TF) of ZnPc and FePc, before and after annealing. Deposited ML and TF spectra of FePc and ZnPc exhibit two main spectral features followed by a low-intensity peak at the

higher binding energy associated to shake-up transition of benzene carbon. The two main peaks are related to the benzene carbon (C_B) at lower BE followed by pyrrole carbon (C_P) peak. Comparison of the binding energy of the different components in the monolayer and the thick film spectra of ZnPc and FePc shows a shift to higher BE for the TF with respect to the ML. This can be explained due to different screening of the molecular film as a function of molecular coverages. Furthermore, the spectral features of the TF of ZnPc are broader and shows a higher shift in BE comparing the ones for the FePc thick film. This can be attributed to different ordering and orientation in the two films leading to different conductivity and screening. The alignment of the molecular films at different coverages is further discussed by XAS measurements.

Figure 6.8 (right panel) shows the carbon 1s core-level photoemission (PE) spectra for the monolayer (ML) and thick films (TF) of ZnPc and FePc after annealing. The ML spectra of ZnPc and FePc are very similar in line shape and BE positions. The annealed TF spectrum of the ZnPc film has shifted more toward lower BE comparing with TF of FePc. We believe that this is due to a thicker FePc film before annealing that partly remains after annealing. Moreover, the spectra at higher BE seem more asymmetric and the intensity of the shake-up transitions has decreased.

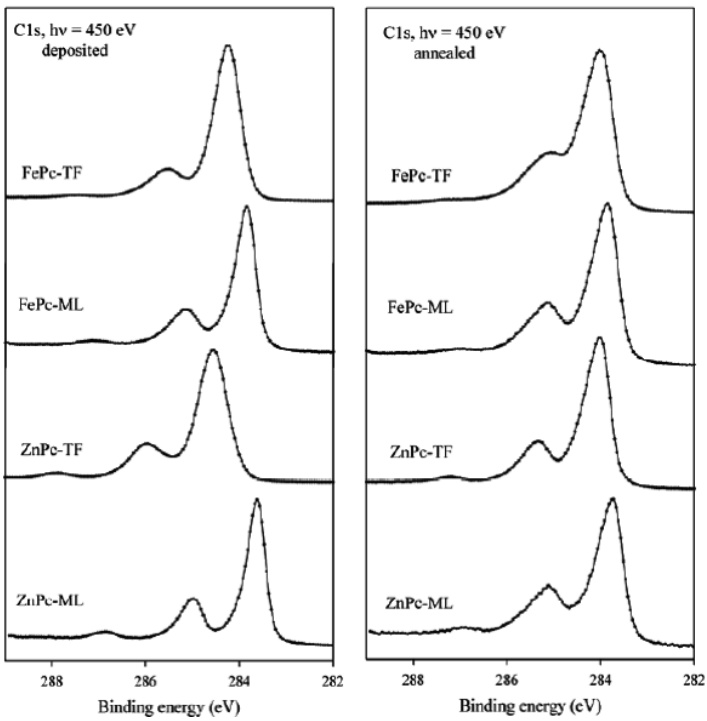

Figure 6.8: C1s spectra recorded from the MPc/Au(111) system at different preparations.

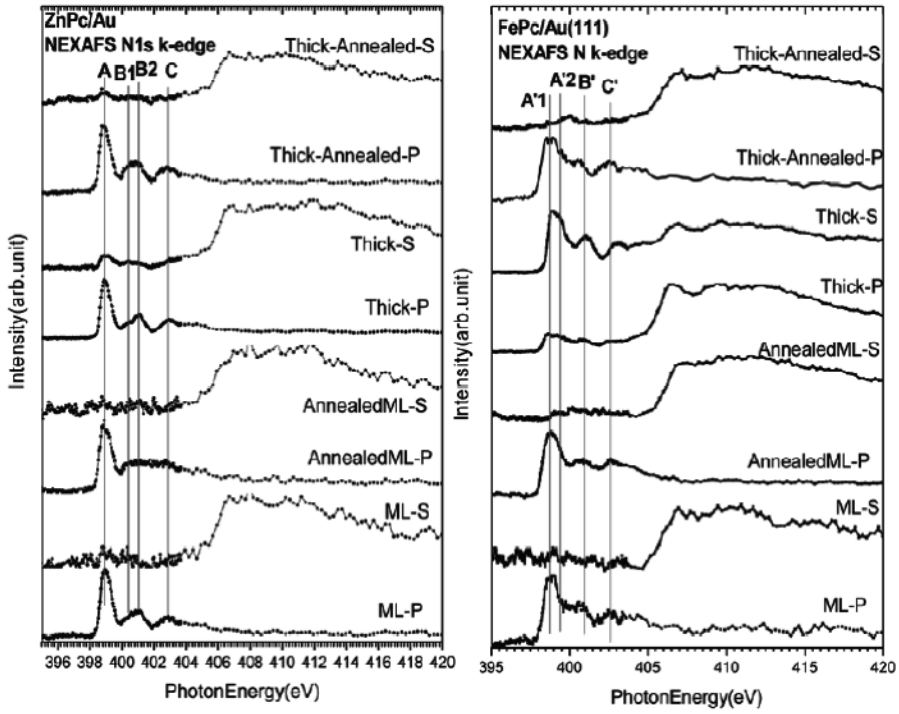

Figure 6.9: N K-edge NEXAFS spectra at different preparations under p and s polarization for (a) ZnPc and (b) FePc molecules on Au(111)

Figure 6.9 presents N K-edge NEXAFS spectra of ML and TF films of ZnPc and FePc on Au(111) before and after annealing. The spectra are measured in two different polarizations; light polarization E vector parallel (s) and orthogonal (p) with respect to the sample surface. Spectra recorded at p-polarization from MLs of FePc and ZnPc are dominated by peaks between 398 eV and 405 eV. The spectrum from the ZnPc monolayer consists of four peaks at photon energies 399.2 eV (A), 400.4 eV (B_1), 401.1 eV (B_2), and finally 402.9 eV (C), whereas the FePc monolayer spectrum has peaks at 398.7 eV (A_1'), at 398.9 eV (A_2') 400.7 eV (B') and 402.4 eV (C'), in a good agreement with literature[74]. These peaks are assigned to the transitions from N1s to unoccupied π^* orbitals with contribution from N2p orbitals. At s-polarization (E vector parallel to the surface) a broader feature is observed at higher photon energy, due to N1s to σ^* transitions. The larger width is due to short life-time of n1s transitions to σ^* excited states[82]. Annealing the monolayers does not change the orientation of the ZnPc and FePc, although a small modification is observed in the line profile of B-C region of ZnPc ML comparing with the same region of the deposited ML. XAS measurements of FePc thick films showed high intensity σ^* features compared to π^* at the experimental geometry of E vector perpendicular to the surface, indicating the standing geometry of the molecular film. Standing of the molecules indicates

stronger molecule-molecule interactions[83]. However, ZnPc thick film remained parallel to the substrate. Parallel alignment of molecular film at the both ML and TF has been observed for studies of H_2Pc on Au(111).
After annealing, the TF film of FePc regains the flat orientation on the surface due to thickness reduction.

Investigation of the valence band of ZnPc and FePc molecules as a function of coverages revealed the effects of central metals on the electronic structures of the films. Figure 6.10 presents the valence band PE spectra of the ZnPc films as a function of molecular coverage before and after annealing as well as close-up spectra around Zn3d and Fermi level.

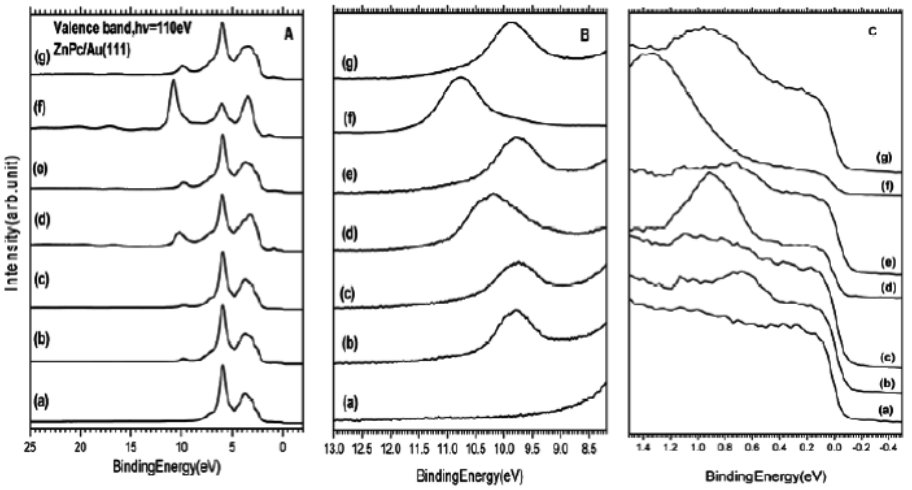

Figure 6.10: Valence band photoemission spectra of ZnPc on Au(111) a) clean Au, b)1ML ZnPc, c) b annealed at 400 °C, d) a few ML, e) d after annealing, f) thick (bulk-like) film, g) f after annealing. The left-hand panel shows overview spectra, the middle panel shows Zn3d and finally the right-hand panel displays the HOMO region near the Fermi level.

Increasing of the molecular coverage causes a shift in Zn3d peak to higher BE, while annealing of the film shifts back the BE of the peak due to change in thickness of the film and different screening of the molecular films.

HOMO of the ML film is observed at 0.8 eV. It shifts to higher BE by increasing the molecular thickness and fully develops to the molecular HOMO at the TF at about 1.35 eV. The HOMO peak becomes broader by annealing of the thick film and a well-ordered monolayer can be found[27].

Figure 6.11 shows the VB spectra of the FePc film as a function of coverage (before and after annealing). The interface-HOMO appears at 0.72 eV at ML coverage and develops to a molecular HOMO at 1.50 eV by increasing the molecular layer thickness. An additional feature in the FePc monolayer spectra at 0.13 eV is observed which does not appear in VB spectra of ZnPc.

The peak has highest intensity at the ML and decreases at higher coverage and disappears in the thick film spectrum. A similar state was observed by Gargiani et al. for FePc on Au(110)[84].

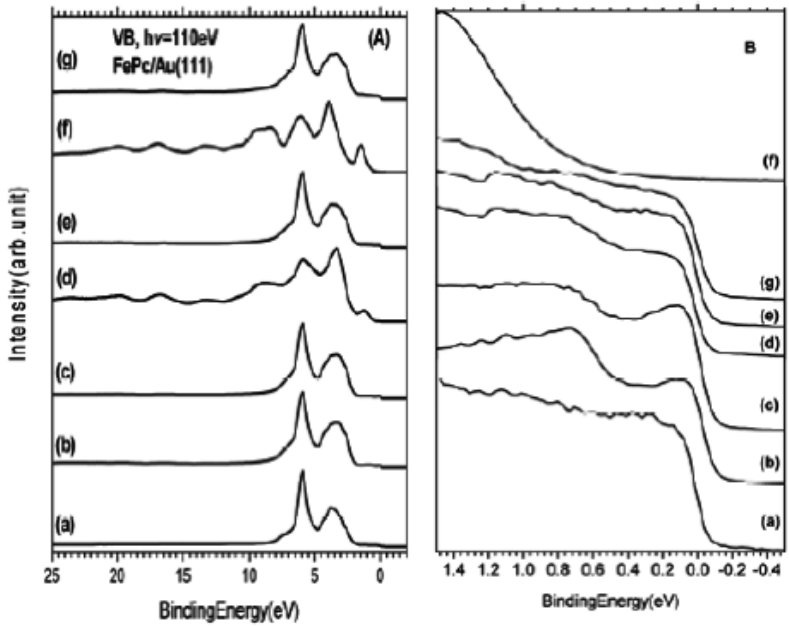

Figure 6.11: Valence band photoemission spectra of FePc on Au(111); a) clean substrate, b) 1 ML FePc, c) 1 ML FePc annealed at 400 °C, d) a few ML, (e) d after annealing, (f) Thick (bulk-like)film, (g) f after annealing. The left hand panel shows overview spectra and the right hand panel focus on the near Fermi level region.

The valence electronic structure of FePc and ZnPc are considerably different. In the FePc molecule, the HOMO and HOMO-1 are very close and are built from contributions of C2p and Fe3*d* orbitals, respectively, while, the HOMO in ZnPc is located on the phthalocyanine ring[85, 86]. Iron has fewer electrons in the d band (d^6), comparing to zinc atom with fully filled *d*-orbital (d^{10}). The electrons in the *d* orbitals take direct part in the interaction with the substrate, which enhances the interaction states close to the Fermi level. Therefore, this state is created due to charge transfer from substrate metal states to the former LUMO (Lowest Unoccupied Molecular Orbital)[84].

Furthermore, we have studied the work function of the clean gold sample and ZnPc and FePc molecular films at different coverages before and after annealing to investigate the charge transfer mechanism. In PES the low energy cut-off determines the work function. After molecule deposition, the cutoff shifts to lower kinetic energy, which translates to a reduced work function according to $\Delta\Phi = \Phi_{Pc} - \Phi_{Au}$[87]. In order to obtain a more clear image of energy level alignment at the interface of Au and Pc molecules, the hole injection barrier (Δ_h) is also investigated which is achieved by measuring the

distance between HOMO edge (linear extrapolation of the low binding energy onset) and the Fermi level. The schematic energy level alignments are presented in Figure 6.12.

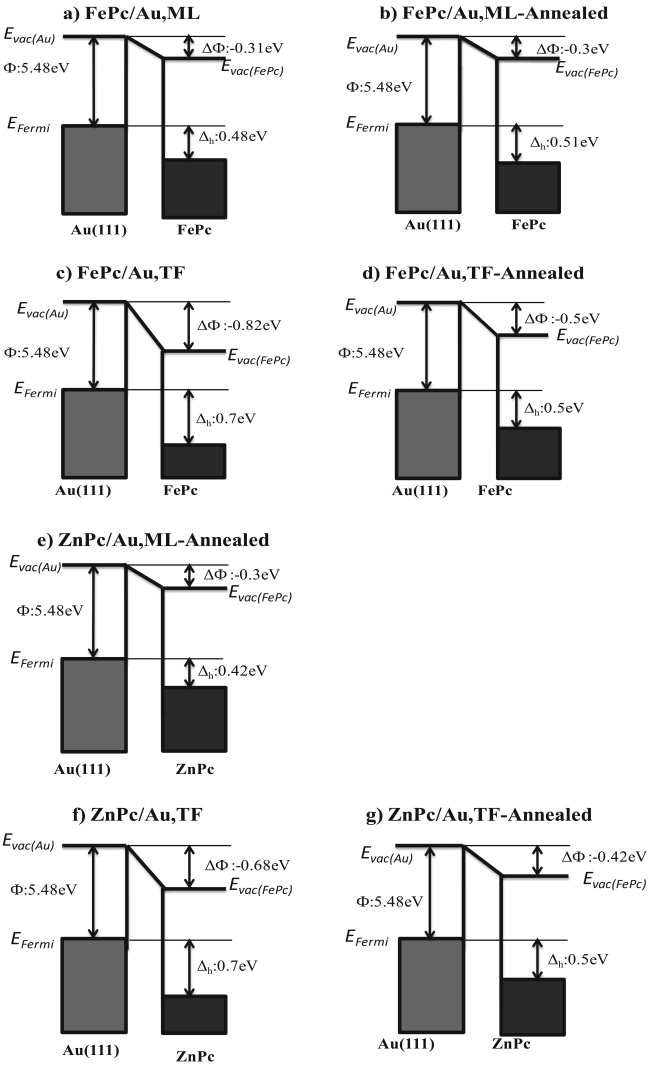

Figure 6.12: Schematic energy level diagrams of FePc/Au(111), (a) monolayer, (b) annealed monolayer, (c) thick film, (d) annealed thick film, and ZnPc/Au(111), (e) annealed monolayer, (f) thick film, and (g) annealed thick film.

Work-function changes combined with valence-band results indicate that both molecules donate charge to Au, however through different channels. The Fe3d derived LUMO (Lowest Unoccupied Molecular Orbital) hybridizes with and receives charge from the substrate when forming an interface state at the Fermi level.

ZnPc donates charge through the π-system, which affects the whole molecule homogeneously, where for FePc the interaction with the surface seems to occur via different channels: π system and the metal center. Thus, the central atom plays an important role in mediating the charge, but the charge transfer as a whole is a balance between different channels.

6.1.4 Investigation of valence band structure of Pc films: A comparison between the metal and metal-free phthalocyanine spectra (paper IV)

Valence band electronic structures of metal-free phthalocyanine have been studied by theoretical simulation and experiment. Comparison of the experimental VB spectrum of H_2Pc/Au(111) with partial and total DFT calculations (Figure 6.13) shows the atomic orbitals that have contributed to the valence band PE spectrum. The overall theoretical spectrum is in excellent agreement with the experimental data. The peaks in experimental data have been labeled from A to I according to our previous work on FePc/Si(100)[74]. The HOMO (Highest Occupied Molecular Orbitals) peak position at 1.5 eV BE (peak A) is in agreement with previous theoretical and experimental studies of a thick film of H_2Pc on conductive glass[26]. It was found from the previous theoretical studies that the HOMO peak is a π orbital formed by C2*p* orbitals[26].

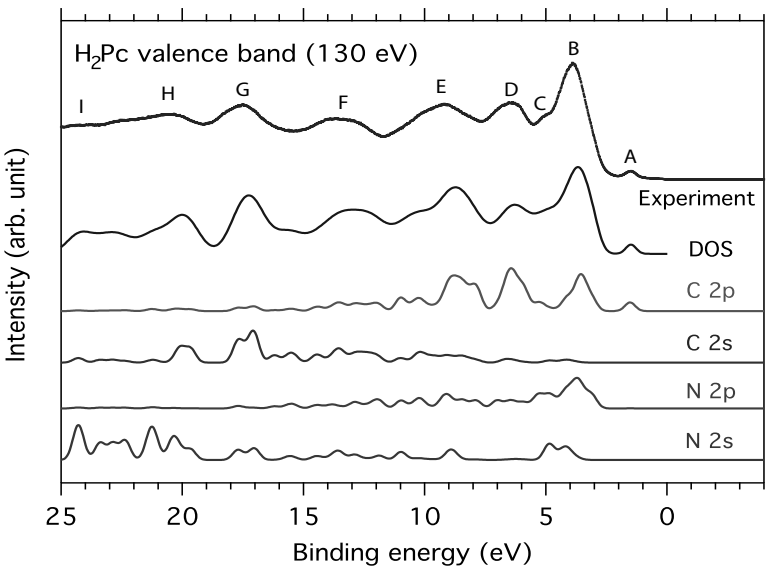

Figure 6.13: Experimental spectrum of a thick film of H_2Pc/Au(111) and DFT calculation of total and partial DOS of a single H_2Pc molecule.

Figure 6.14 shows the experimental valence band spectra of FePc in gas-phase, FePc/Si(100) film together with simulated spectrum of a single FePc molecule. In the spectrum of FePc film the HOMO gives rise to a broad peak at about 1.8 eV BE, while two spectral features are presented in the gas phase. This is also reproduced in the simulated spectrum at 1.2 eV and 1.8 eV BE and more details are presented in inset. It was discussed in our gas-phase studies of FePc that the HOMO peak at 1.2 eV is due to C 2p whereas the HOMO-1 feature at 1.8 eV is related to Fe3d contributions[68]. These spectral features converge in a single broad peak at 1.8 eV in the film spectrum.

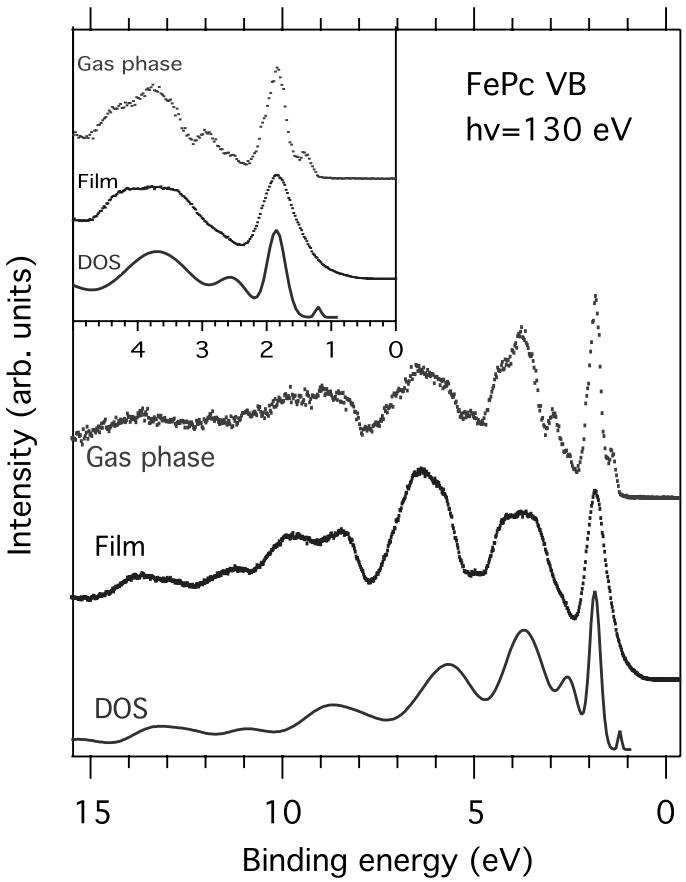

Figure 6.14: Experimental spectrum of FePc in gas phase, a thick film of FePc/Si(100) and DFT calculation of total DOS of a single H_2Pc molecule.

The difference in contribution of the HOMO and HOMO-1 spectral features for the FePc spectrum becomes evident by comparison of the valence spectra of H_2Pc and FePc together with FePc gas-phase data (Figure 6.15). It is ob-

served that the HOMO of the H_2Pc and FePc films (in both cases due to C2p contributions) are almost at the same BE.

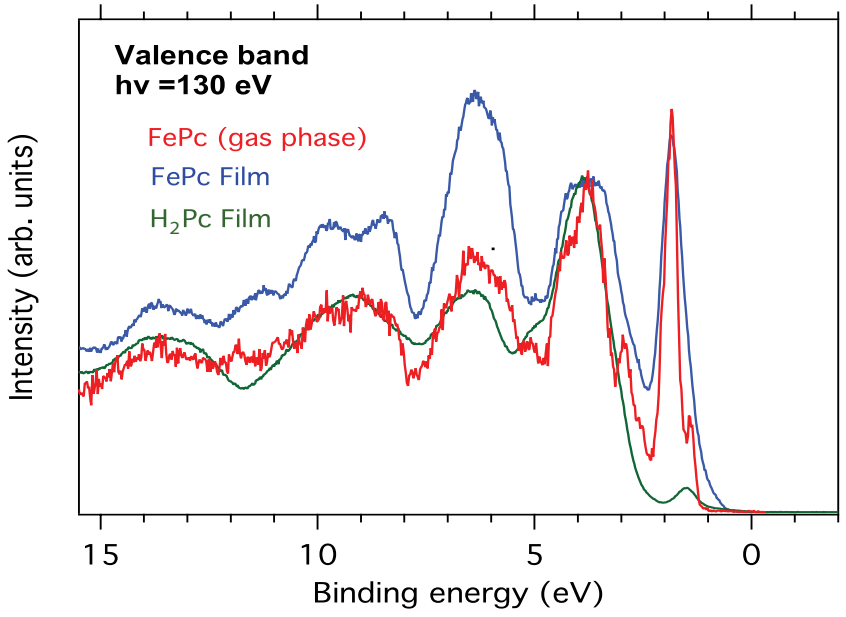

Figure 6.15: Comparison between the spectra of thick films of FePc/Si(100) and H_2Pc/Au(111) and FePc in gas-phase.

6.2. Modification of the geometric and electronic properties of Pc molecules after alkali doping

As mentioned earlier, modification of the electronic properties of molecular films by introducing charge donation or acceptance from a dopant is fundamental to understand charge transport in these molecular systems[35, 88]. In recent years, many theoretical and experimental studies have been performed on modification of the electronic properties of MPcs molecular films as a function of metal alkali intercalation[79, 89, 90]. An insulator-to-metal transition of Pcs has been predicted by theoretical[79] and experimental[35] studies. However, no metallic phase has been observed at any doping level of alkali metal in any experimental reports to verify this prediction. In this work, we have investigated the modification of metal-free phthalocyanine (H_2Pc) deposited on metal substrates and doped by alkali dopant. The lack of a metallic center may largely influence the geometric arrangement of the alkali atoms and alter the electronic and geometric structure of the molecules. Low-temperature STM studies have been performed to image geometric arrangement of the molecular monolayer after Rb doping. Photoelectron Spectros-

copy (PES) has been used to map the electronic core and valence levels. X-ray Absorption Spectroscopy (XAS) has also been used, which provides a direct characterization of how the unoccupied molecular orbitals of H_2Pc are affected by K intercalation. In addition, theoretical calculations have been done to support our experimental data.

6.2.1. Rubidium doped metal-free phthalocyanine monolayer on Au(111) (paper I)

Rubidium doping of H_2Pc monolayer on Au(111) $\left(\sqrt{3} \times 22\right)$ reconstructed surface has been investigated by low temperature (LT) Scanning Tunneling Microscopy at 70 K. Figure 6.16 displays the co-adsorbed system characterized by Rb-induced bright protrusions observed on top of the molecular layer, resulting in a well-ordered system with pairs of bright protrusions evenly distributed over the surface. However, a single bright protrusion is observed in few cases, indicated by a white ellipse in the figure.

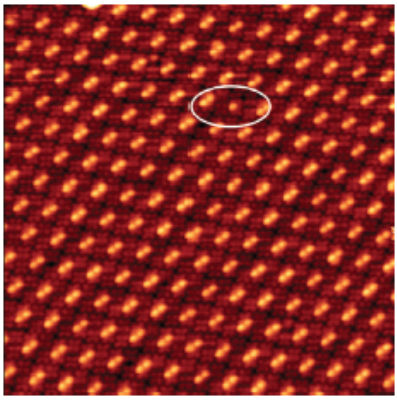

Figure 6.16: LT STM image (-2.61 V, 0.14 nA, 37.8 nm × 37.8 nm) of a H_2Pc monolayer on Au(111) surface, doped with Rb

Investigation of the protrusion position with respect to the H_2Pc layer on different places of the sample reveals that the Rb pairs are located on top of one of the Pc benzene rings in two adjacent molecules, which clearly indicates that the Rb is not interacting with the H_2Pc molecular center. In fact, STM images do not show any sign of metallization of the molecules, as the central ring of the macrocycle was always imaged as a dip, independently of the bias used. This is different from for example the study dedicated to the metallization of H_2Pc by Fe, which instead fits in the molecular center[91]. The different behaviors observed for Fe and Rb can most likely be explained by the different electronic structure of the two metals, as well as by simple geometric considerations as the radius of the alkaline ion would probably not

fit in the molecular center. Furthermore, the metallic center in a MPc is usually in a ionic state with charge +2 while alkali are usually forming a ionic state with charge +1.

Rb doping of the H_2Pc monolayer also modifies significantly the molecular adsorption geometry. Figure 6.17 shows a comparison between undoped and Rb-doped H_2Pc/Au(111) system. As discussed in the previous section the H_2Pc/Au(111) system is characterized by a square unit cell, with 1 molecule per unit cell, whereas the Rb/H_2Pc/Au(111) system displays a hexagonal unit cell, with 4 molecules per unit cell.

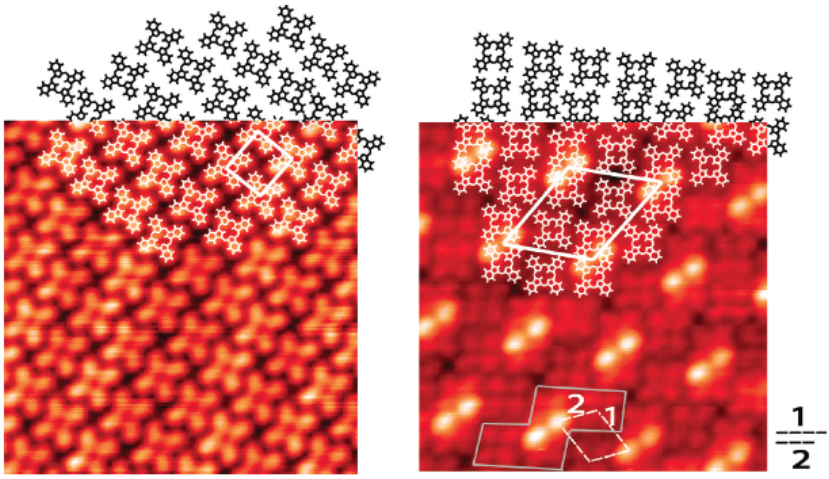

Figure 6.17: (Left) H_2Pc/Au(111) (-1.45 V, 0.17 nA, and 10.4 × 10.4 nm). (Right) Rb-doped H_2Pc on Au(111) (-2.62 V, 0.14 nA, and 10.4 ×10.4 nm). The molecular adsorption unit cells are indicated by white lines and schematic models marks the positions of single directions.

Comparing the length of the unit vectors for both systems reveals that the H_2Pc molecules are slightly more densely packed (about 10%) after Rb doping. The geometric arrangement of the H_2Pc molecules, with respect to their nearest neighbors, is highly affected by the Rb doping. The former arrangement with the benzene group of one molecule close to an aza-bridging nitrogen atom in the neighboring molecule is no longer observed. In the hexagonal molecular adsorption unit cell, after Rb doping, the molecules are instead arranged with the benzene groups of neighboring molecules close to each other. Moreover, in the latter case, the distances between neighboring molecules are significantly different along different directions. As seen in the right-hand side of Figure 6.10, the molecules are arranged so that they are closer toward one of the pair of bright protrusion.

It is concluded that the interactions in the system are significantly changed after Rb doping. The balance between adsorbate-adsorbate and ad-

sorbate-substrate interactions in the doped system results in a modified molecular adsorption structure as compared to the pristine system.

6.2.2. Potassium doped metal-free phthalocyanine multilayer films on Al(110) (paper V)

The electronic structure of the H_2Pc films on Al(110) as a function of potassium intercalation has been studied by photoelectron spectroscopy. PES measurements reveal the presence of several charge states of the molecules upon K doping, due to charge transfer from the alkali to the molecular film. Figure 6.18 (left panel) shows C1s and K2p spectra of the pristine H_2Pc film and the films at different K doping levels. A shift towards higher binding energy is observed in all features of the C1s spectra due to shift of the Fermi level position. The shift of Fermi level positions is ascribed to the filling of initially empty states upon charge transfer from the alkali atoms.

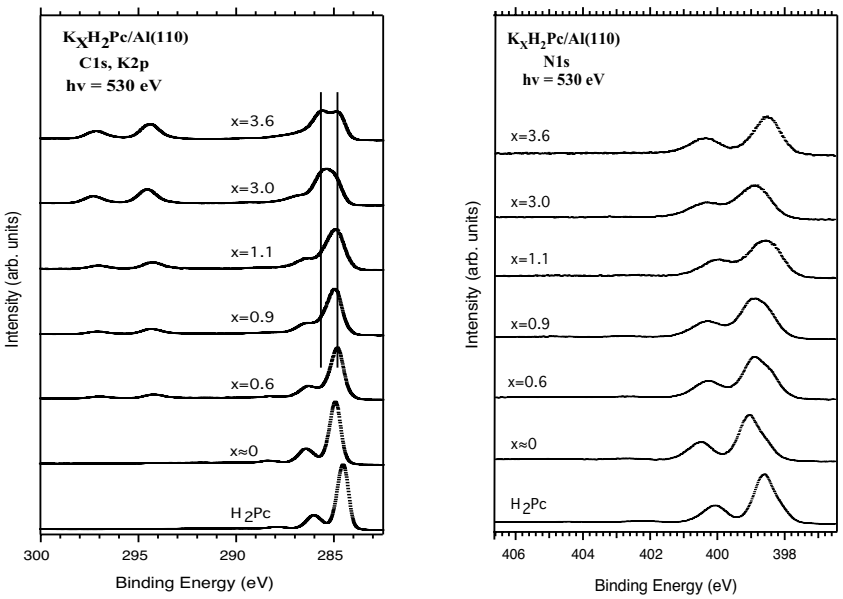

Figure 6.18: C1s, K2p and N1s PE spectra of the pristine H_2Pc film and the films after exposing to different doses of potassium.

With increasing the K dose, the line shape becomes broader and two peaks at the higher BE are observed, which are related to $K2p_{3/2}$ and $K2p_{1/2}$ photoemission lines at 294.1 eV and 297.1 eV BE, respectively. Moreover, no shake-up peak has been observed at a doping level of x=0.9 and higher doses.

N1s spectra of the pristine H_2Pc film and the films after different K doping levels are presented in the right panel of Figure 6.11. An asymmetry in the line shape and a shift toward higher BE are observed for the doped films due to charge transfer from the alkali metal and filling of the initially empty states.

Observation of changes in the line profile and width of the C1s and N1s spectral lines are similar to previous studies of MPc as a function of alkali metal intercalation[39, 40]. These changes were attributed to a lowering of the molecular symmetry caused by the adsorption sites. It was proposed in the studies of K on FePc that the alkali atoms would form two different stoichiometric phases, namely K_2Pc and K_4Pc depending on the alkali interaction (ref)[92]. However, for other MPc like MnPc some investigations have proposed additional phase formation, namely KMPc phase. In our studies, the broadening of the N1s line profile for different potassium doses indicates that the pyrrole atoms are probably the most affected by alkali adsorption. Furthermore, we cannot neglect a remarkable broadening of the peak related to the benzene-like carbon atoms.

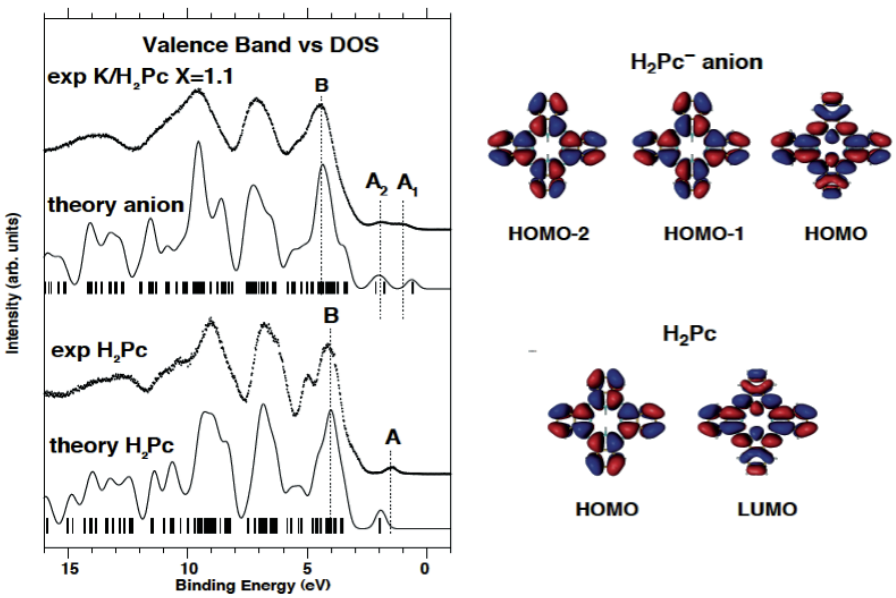

Figure 6.19: (left panel) Comparison of experimental valence band PE spectra for pristine and K-intercalated film (solid lines represent the theoretical simulation of the spectra considering a single H_2Pc molecule and an anion H_2Pc^-). (Right panel) DFT simulation picture of HOMO and LUMO of a single H_2Pc molecule and HOMO-2, HOMO-1 and HOMO of H_2Pc^- anion. The images show the similarity between the HOMO of the anion and the LUMO of the pristine H_2Pc.

Comparison of the valence band spectra and DFT calculations of the density of states of the H_2Pc anion indicates a filling of lowest unoccupied molecular orbital (LUMO) by charge transfer from the alkali. Experimental valence band PE spectra for pristine and K-intercalation H_2Pc films are presented in the left panel of Figure 6.19, which indicates that the HOMO peak of the pristine film (peak A), has been split into two sub-peaks of A1 and A2 after K doping. These peaks are well described by DFT calculations of orbital pictures of HOMO and LUMO of a single H_2Pc molecule that has been compared with HOMO-2, HOMO-1 and HOMO of a H_2Pc^- anion (Figure 6.19, right panel). The addition of one electron to the molecule when forming the H_2Pc^- anion lifts the spin degeneracy of the electronic states. The extra electron of the negative ion occupies the empty LUMO orbitals of the neutral H_2Pc molecule. The HOMO of the anion is very similar to the LUMO of the neutral H_2Pc, confirming that the new peak at the lowest BE in the valence band PE spectrum of the intercalated films is due to the occupancy of the molecular LUMO (now anion HOMO) by the alkali electron transfer. This has been further confirmed by XAS studies, which showed a decreased density of unoccupied states.

Figure 6.20 shows N1s XA spectra of the pristine and K-intercalated film in the experimental geometry of the E vector of the incoming light parallel to the surface. The spectra show the reorientation of the molecular film after K doping.

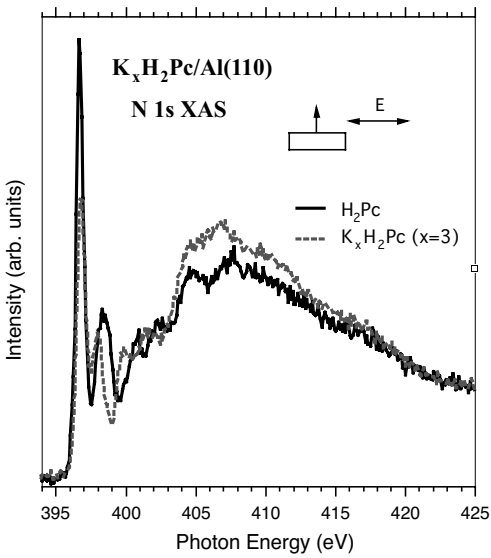

Figure 6.20: N1s X-ray absorption spectra of a pristine H_2Pc and a film intercalated with K at experimental geometry of the E vector parallel to the surface.

N1s and C1s XAS (Figure 6.21) measurements in different experimental geometries reveal that the molecules in the pristine film are standing upright on the surface or are only slightly tilted away from the surface normal, but after K intercalation the molecular orientation is changed in that the tilt angle of the molecules is increased.

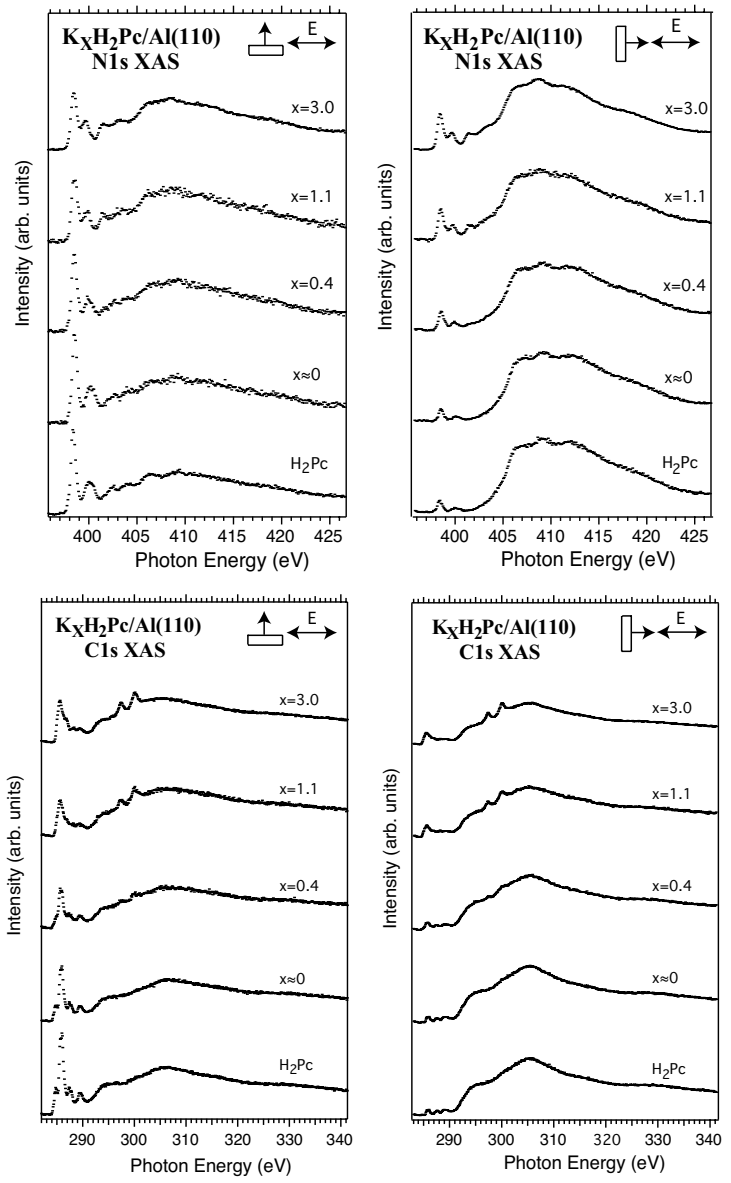

Figure 6.21: N1s and C1s XA spectra of the pristine H_2Pc film and different K intercalated films. The spectra have been recorded at two experimental geometries, in which the E vector of the incoming light was parallel (left panels) and perpendicular (right panels) to the surface.

7. Summary and outlook

In this thesis, adsorption of monolayers and multilayers of metal-free and metal phthalocyanines molecules on metal surfaces has been investigated using complementary spectroscopic and microscopic techniques.

It was observed by STM measurements that at monolayer coverage the adsorption direction of the metal-free phthalocyanine molecules with respect to the gold surface varies as a function of temperature, i.e. at RT and LT. It was explained by the difference in strength of intermolecular and adsorbate-substrate interactions at room and low temperatures.

XPS measurements have provided further information on the nature of the interaction between adsorbed species and the surfaces as a function of coverage.

The alignment of molecular films at both monolayer and multilayer coverages, which has been determined by XAS measurements in several cases, is also dependent upon the relative strength of molecule-molecule versus molecule-substrate interaction. Parallel alignment of the molecular film with respect to the surface is the result of significant interaction between the adsorbate and the substrate, whilst standing geometry of the molecular film is due to more significant intermolecular interactions.

Moreover, investigation of alkali interaction of the phthalocyanine films revealed a significant modification in their geometric and electronic structures due to charge transfer from the alkali metal to the molecular film. However, no sign of metallization of the molecules has been observed by spectroscopic and microscopic studies.

Phthalocyanine molecules have been extensively studied in the last two decades due to their possible application in organic solar cells, organic light-emitting devices and gas sensors. High performance and efficiency of such devices needs a better understanding of the electronic and geometric properties and parameters that affects these properties. Therefore, there are plenty of rooms for future investigations. In our opinion, in future new experimental methods will be developed allowing to characterize such molecular films under working conditions. This will include study of catalytic performance, gas sensing and pump probe investigations.

8. Populärvetenskaplig sammanfattning

Organiska molekyler kan användas som material med små bandgap och kan därmed fungera som aktiva lager i komponenter som finns i organiska solceller eller organiska ljusdioder (OLED:s). Det är således viktigt att undersöka den hur elektronerna rör sig i tunna filmer av organiska molekyler, och hur laddning transporteras över gränsytor i sådana filmer. Vi behöver denna kunskap för att kunna förbättra komponenternas elektroniska och optiska egenskaper. Det är också viktigt att kunna studera molekylära filmer som täcker ytor på olika sätt - utgör de monolager eller finns det fler lager i filmen? Man måste även kunna beskriva hur laddningar transporteras om man vill kunna utveckla och kontrollera komponenter av molekylära material. Ett annat område för forskning utgörs av hur filmen växelverkar med substratet som det lagts ut på. Slutligen är det avgörande att kunna modifiera elektronstrukturen genom att introducera dopningsämnen för att ändra på laddningstransportsegenskaperna.

Röntgenbaserad fotoelektronspektroskopi (XPS) och röntgensabsorptions-spektroskopi (XAS) är två mycket kraftfulla tekniker vi använder oss av för att erhålla information om hur elektronerna fördelar sig på fyllda och tomma kvanttillstånd i substratet och i den adsorberade molekylära filmen. XAS kan dessutom användas till att studera hur molekylerna ligger ordnade geometriskt på substratets yta. Här har man stor användning av de nya generationer av s.k. synkrotronljusanläggningar som levererar oerhört högbriljanta, avstämbara och polariserade röntgenstrålar. Genom att kombinera dessa bättre röntgenkällor med högteknologiska mätutrustningar kan vi få mycket exaktare och högupplösta data som ger oss en mycket god bild av de kemiska och fysikaliska processer som äger rum på de studerade ytorna och gränsskikten.

Ftalocyaniner (Pc) molekyler är makrocykliska kemiska föreningar som studerats intensivt de senaste åren. Intresset för detta motiveras av de möjligheter vi har att använda dem i olika sammanhang. Dessa molekyler används ofta som färgämnen och man kan också se dem som modellmolekyler som studeras för att förstå mer komplexa biologiska system och processer. Detta låter sig göras eftersom Pc molekylerna liknar biomolekyler som porfyriner, hemoglobin och klorofyll. Pc molekyler är även intressanta att användas i organiska solceller och i organiska ljusemitterande fotodioder. De kan också fungera som aktiva komponenter i kemiska sensorer,

t.ex. gassensorer, och de har också sedan länge framgångsrikt utnyttjats för homogen och heterogen katalys av oxidationsreaktioner.

I denna avhandling har jag huvudsakligen studerat sambandet mellan molekylfilmernas egenskaper och varierat de olika typerna av molekylära lager. Jag har även ändrat styrkan på växelverkan mellan molekylfilmerna och de respektive substratytorna, samt studerat hur temperaturen inverkat på respektive intermolekylär- och adsorbatväxelverkan. Dessutom presenteras studier av hur laddningstransport och elektroniska egenskaper ändras när Pc molekyler dopas med alkalimetaller.

Acknowledgment

Four years passed quickly since I have started my PhD. Doctoral studies have brought me a great experience and transformation, both in my education and personal life. It gave me a chance to advent more independently and of course to know myself better. To know my strengths and weaknesses! In fact, it was not possible to manage it without guidance and supports of my supervisors, friends and family.

This thesis is achievement of a group work. First of all, I would like to thank my supervisors Prof. Maria Novella Piancastelli and Dr. Carla Puglia for all of their helps, supports and encouragements. Maria Novella is a source of knowledge and very kind person. I never forget the night shift-beamtime you stood by me the whole night and support the work. Carla is a creative and intelligent person. I appreciate her for being available for me the time that I needed her guidance and consults despite her tight work schedule.

I would like to appreciate my former supervisors Dr. Emmanuelle Göthelid and Dr. Pål Palmgren for all their patience to teach me technical part of the work and their excellent scientific discussions. I enjoyed working with these excellent scientists and have the best wishes for them in their career and life.

A great thank to Dr. Barbara Brena and Johann Lüder for their fantastic theoretical simulations and scientific discussions.

I gratefully acknowledge Ieva Bidermane, Prof. Mats Göthelid and Sareh Ahmadi whom I have collaborated with. It is my pleasure to work with these excellent people.

I would like to thank Prof. Svante Svensson for his guidance and nice discussion about culture and science. I appreciate him for Swedish translation of popular scientific summary of my thesis.

I would like to thank my former supervisors in Iran Dr. Mahmood Ghoranneviss and Dr. Mohammad Reza Hantehzadeh for all things they taught me. Without their guidance, I might never have the chance to continue my education.

I would like to thank Max-lab staff, especially the beamline managers at I511, Dr. Franz Hennies and Dr. Annette Pietzsch.

I would like to thank all my friends in Iran and Sweden. A great thank to my colleagues and friends in Uppsala University. Rebecka, Johan, Ieva, Josephina, Tiger (Yixiao), Ronny, Davide, Atieh, Johan. S, Joachim, Andreas and Stefan, thanks for your company and friendship.

I am grateful and appreciate you, Tommy, for all your love and supports. I am glad and lucky to have you and your lovely family.

Finally, I would like to thank my parents. With honor, I dedicate my dissertation to my mother. You have been a solid support for me and encouraged me for higher education. Thanks to you for believing me and help me to get my goals. I am grateful and appreciate my sister and brother for all their love and supports. Long distance between us cannot affect and change my love to you. You are always close to me in my heart. I love you very much.

Bibliography

[1] P. Peumans, A. Yakimov, and S. R. Forrest, J. Appl. Phys. **93**, 3693 (2003)
[2] L. S. Hung, and C. H. Chen, Mater. Sci. Eng. R **39**, 143 (2002)
[3] D. Cahen, A. Kahn, and E. Umbach, Mater. Today **8**, 32 (2005)
[4] N. Koch, J. Phys.:Condens. Matter **20**, 184008 (2008)
[5] L. Giovanelli, P. Amsalem, T. Angot, L. Petaccia, S. Gorovikov, L. Porte, A. Goldoni, and J. –M. Themlin, Phys. Rev. B 82, 125431 (2010)
[6] G. Binning and H. Rohrer, Helv. Phys.Acta. **55**, 726 (1982)
[7] D. Attwood, "Soft X-rays and Extreme Ultraviolet Radiation, Principles and Applications", Cambridge (1999)
[8] O. L. Kaliya, E. A. Lukyanet and G. N. Vorozhtsov, J. Porphyr. Phthalocyanines **3**, 592 (1999)
[9] C. K. Mathews, K.E. van Holde and K. G. Ahren, "Biochemistry", 3rd eddition (Addison Wesley Longman, San Francisco, 2000)
[10] Collins, R. A.; Mohammed, K. A. J. Phys. D **21**, 142 (1988)
[11] Hamann, C.; Hietschold, M.; Mrwa, A.; Mueller, M.; Starke, M.; Kilper, R. Top. Organ. Eng. **7**, 129 (1991)
[12] S. Berner, S. Biela, G. Ledung, A. Gogoll, J. –E, Bäckvall, C. Puglia and S. Oscarsson, J. Catalysis, **244**, 86 (2006)
[13] E. Higurashi, D. Chino, T. Suga, Member, IEEE and R. Sawada, IEEE Journal of selected topics in quantum electronics, **15**, 5 (2009)
[14] P. Maksymovych, O. Voznyy, D. B. Dougherty, D. C. Sorescu and J. T. Y. Jr, Prog. in Surfa. Sci. **85**, 206 (2010)
[15] T. Li, W. Hu and D. Zhu, Adv. Mater. **21**, 1 (2009)
[16] B.K. Min, A.R. Alemozafar, M.M. Biener, J. Biener, and C.M. Friend, Topics in Catalysis **36**, 77 (2005)
[17] James D. Plummer, Michael D. Deal, and Peter B. Griffin, "Silicon VLSI Technology, Fundamentals, Practice and Models", Prentice Hall, Upper Saddle River, NJ.(2000)
[18] K. L. Chopra, P. D. Paulson, and V. Dutta, Prog. Photovolt: Res. Appl. **12**, 69-92 (2004)
[19] M. Thelakkat, C. Schmitz, and H.-W. Schemidt, Adv. Mater. (Weiiheim, Ger) **14**, 577 (2002)
[20] J. C. Conboy, E. J. C. Olson, D.M. Adams, J. Kerimo, A. Zaban, B. A. Gregg, and P. E. Barbara, J. Phys. Chem. B. **102**, 4516 (1998)
[21] M. Trometer, R. Even, J. Simon et al., Sens. Actuators B **8**, 129 (1992)
[22] A. A. Kuznetsov, V. I. Filippov, R. N. Alyautdin, N. L. Torshina, and O. A. Kuznetsov, J. Magn. Magn. Mater. **225**, 95 (2001)
[23] D. Hohnholz, S. Steinbrecher, and M. Hanack, J. Mol. Struct. 521, 231 (2000)
[24] Y. –S. Huang, J. –H. Jou, W. –K. Weng, and J. –M. Liu, Appl. Phys. Lett. **80**, 2782 (2002)

[25] S. Heutz, C. Mitra, W. Wu, A. J. Fisher, A. Kerridge, M. Stoneham, T. H. Harker, J. Gardener, H. –H. Tseng, T. S. Jones, C. Renner, and G. Aeppli, Adv. Mater. **19**, 3618-3622 (2007)
[26] Y. Alfredsson, B. Brena, K. Nilson, J. Åhlund, L. Kjeldgaard, M. Nyberg, Y. Luo, N. Mårtensson, A. Sandell, C. Puglia, and H. Siegbahn, J. Chem. Phys. **122**, 214723 (2005)
[27] K. Nilson, J. Åhlund, M. -N. Shariati, E. Göthelid, P. Palmgren, J. Schiessling, S. Berner, N. Mårtensson, and C. Puglia, J. Phys. Chem. C, **114** (28), 12166-12172 (2010)
[28] S. M. Critchley, M. R. Willis, M. J. Cook, J. McMurdo and Y. Maruyama, J. Mater. Chem. **2**, 157 (1992)
[29] T. R. E. Simpson, D. J. Revell, M. J. Cook, and D. A. Russell, Langmuir, **13 (3)**, 460 (1997)
[30] J. H. Sharp and M. Lardon, J. Phys. Chem. **72**, 3230 (1968)
[31] D. Verma, R. Dash, K. S. Katti, D. L. Schulz and A. N. Caruso, Spectrochimica Acta Part A **70**, 1180-1186 (2008)
[32] F. Iwatsu, J. Phys. Chem. **92**, 1678 (1988)
[33] K. Oka, O. Okada, J. Imaging Sci, Technol. **37**, 13 (1993)
[34] K. Walzer, B. Maeninh, M. Pfeiffer, and K. Leo, Chem. Rev. **107**, 1233-1271 (2007)
[35] M. F. Cracium, S. Roggr, M._J. L.den Bor, S. Margadonna, K. Prassides, Y. Iwasa, and A. F. Morpurgo, Adv. Mater. **18**, 320-324 (2006)
[36] H. Ding, K. Park, K. Green, and Y. Gao, Chem. Phys. Lett. **454**, 229-232 (2008)
[37] M. F. Cracium, S. Roggr, and A. F. Morpurgo, J. Am. Chem. Soc. **127**, 12210-12211 (2005)
[38] P. Gargiani, A. Calabrese, C. Mariani, and M. G. Betti, J. Phy. Chem. C **114**, 12258-12264 (2010)
[39] V. Yu. Aristov, O. V. Molodtsova, V. V. Maslyuk, D. V. Vyalikh, T. Bredow, I. Mertig, A. B. Preobrajenski, and M. Knupfer, J. Org. Elect. **11**, 1461-1468 (2010)
[40] O. V. Molodtsova, V. M. Zhilin, D. V. Vyalikh, V. Yu. Aristov and M. Knupfer, J. Appl. Phys. **98**, 09702 (2005)
[41] K.W. Kolasinski, "Surface Science", John Wiley and sons (2001)
[42] H. Lüth, "Solid Surfaces, Interfaces and Thin Films", Fourth edition, Springer (2001)
[43] C. Argile, G. E. Rhead, Surf. Sci. Rep. **10**, 277 (1989)
[44] J. A. Venables, J. Vac. Sci. Technol. B **4(4)**, 870 (1986)
[45] E. Bauer, H. Poppa, Thin Solid Films **12**,167 (1972)
[46] A. Einstein, Ann. Phys. **17**, 132 (1905)
[47] K.Siegbahn, C. Nordling, A. Fahlman, R. Nordberg, K. Hamrin, J. Hedman, G. Johansson, T. Bergmark, S.E. Karlsson, I. Lindgren and B. Lindgren, ESCA Atomic, Molecular and Solid State Structure Studied by means of Electron Spectroscopy (Almqvist och Wiksells Boktryckeri AB, Uppsala, 1967)
[48] M. P. Seah, W. A. Dench, Surf. Interface. Anal. **1**, 2 (1979)
[49] W. Ebergang, N. Mårtensson, A. Nilsson "Application of Synchrotron Radiation: High-Resolution Studies of Molecules and Molecular Adsorbates on Surfaces", Springer Series in Surface Science, Vol. **35** (1994)
[50] C. R.Brundle, A. D. Baker, "Electron Spectroscopy: Theory, Techniques and Applications" Vol.**2**, Academic press (1978)

[51] N. Mårtensson, "Core level Spectroscopies Applied to Surface and Adsorbates", lecture notes (1994)
[52] A. Nilsson, O. Björneholm, E. O. F. Zdansky, H. Tillborg, N. Mårtensson, J. N. Andersen, and R. Nyholm, Chem. Phys. Lett, **197**, 12 (1992)
[53] C. Puglia, A. Nilsson, B. Hernnäs, O. Karis, P. Bennich, and N. Mårtensson, Surf. Sci. **342**, 119-133 (1995)
[54] B. Brena, Y. Luo, M. Nyberg, S. Carniato, K. Nilson, Y. Alfredsson, J. Åhlund, N. Mårtensson, H. Siegbahn and C. Puglia, Phys. Rev. B **70**, 195214 (2004)
[55] B.H. Brandsen and C.J. Joachain, "Introduction to Quantum Mechanics" (Addison-Wesley Longman, Edingburgh Gate, 1989)
[56] W. Kossel, Z. Phys. **1**, 119 (1920); ibid. **2**, 470 (1920)
[57] J. Stöhr, NEXAFS Spectroscopy (Springer-Verlag, Berlin, 1992)
[58] J. Adachi, N. Kosugi and A. Yagishita, J. Phys. B **38**, R127 (2005)
[59] G. Binning, H. Rohrer, C. Gerber and E. Weibel, Phys. Rev. Lett. 49, 57 (1982)
[60] J. Repp, G. Meyer, F.E. Olsson, and M. Persson, Science **305**, 493 (2004)
[61] J. Repp, G. Meyer, S. Stojkovic, A. Gourdon, C. Joachim, Phys. Rev.Lett. **94**, 026803 (2005)
[62] D.M. Eigler, E. K. Schweizer, Nature **344**, 524 (1990)
[63] R. Young, J. Ward, and F. Scire, Phys. Rev. Lett. **27**, 922 (1971)
[64] E. Meyer, H. J. Hug and R. Bennewitz, "Scanning Probe Microscopy, The Lab on a Tip", Springer (2003)
[65] Xing Lu and K. W. Hipps, J. Phys. Chem. B, **101** (27), 5391 (1997)
[66] M. Wakisaka, Sh. Asizawa, H. Uchida and M. Watanabe, Phys. Chem. Chem. Phys. **12**, 4184 (2010)
[67] N. Argaman and G. Makov, arXiv:physics/9806013v2 (1999)
[68] B. Brena, C. Puglia, M. de Simone, M. Coreno, K. Tarafder, V. Feyer, R. Banerjee, E. Göthelid, B. Sanyal, P. M. Oppeneer, and O. Eriksson, J. Chem. Phys. **134**, 074312 (2011)
[69] R. Denecke, P. Väterlein, M. Bässler, N. Wassdal, S. Butorin, A. Nilsson, J. –E. Rubensson, J. Nordgren, N. Mårtensson, and R. Nyholm, J. Electron Spectrosc. Relat. Phenom. **971**, 101-103 (1999)
[70] Z.H. Cheng, L. Gao, Z. T. Deng, Q. Liu, N. Jiang, X. Lin, X. B. He, S. X. Du, and H.-J. Gao, J. Phys. Chem. C, **111**, 2656 (2007)
[71] I. Chizhov, G. Scoles, and A. Kahn, Langmuir **16**, 4358-4361 (2000)
[72] M. Takada and H. Tada, Chem. Phys. Lett. **392**, 265-269 (2004)
[73] K. Nilson, J. Åhlund, B. Brena, E. Göthelid, J. Schiessling, N. Mårtensson and C. Puglia, J. Chem. Phys. **127**, 114702 (2007)
[74] J. Åhlund, K. Nilson, J. Kjeldgaard, S. Berner, N. Mårtensson, C. Puglia, B. Brena, M. Nyberg, and Y. Luo . J. Chem. Phys. **125**, 34709 (2006)
[75] P. Palmgren, B. R. Priya, N. P. P. Nirya and M. Göthelid, J. Phys. Cond. Mater. **18**, 10707 (2006)
[76] K. Nilson, P. Palmgren, J. Åhlund, J. Schiessling, E. Göthelid, N. Mårtensson, C. Puglia and M. Göthelid, Surf. Sci. **602**, 452–459 (2008)
[77] P. Palmgren, B. R. Priya, N. P. P. Nirya and M. Göthelid, J. Solar Energy. Mater and Solar Cells. **90**, 3602-3613 (2006)
[78] G. Dufour, C. Poncey, F. Rochet, H. Roulet, M. Sacchi, M. De Santis, M. De Crescenzi, Surf. Sci. **319**, 251 (1994)
[79] E. Tosatti, M. Fabrizio, J. Tóbik , and G. E. Santoro, Phys. Rev. Lett. **93**, 117002 (2004)

[80] Z.H. Cheng, L. Gao, Z. T. Deng, N. Jiang, Q. Liu, D. X. Shi, S. X. Du, H. M. Guo, and H.-J. Gao, J. Phys. Chem. C, **111**, 9240 (2007)

[81] C. Puglia, P. Bennich, J. Hasselström, C. Ribbing, P.A. Brühwiler, A. Nilsson, Z. Y. Li and N. Mårtensson, Surf. Sci. **414**, 118-130 (1998)

[82] O.V. Molodtsova, M. Knupfer, V.V. Maslyuk, D.V. Vyalikh, V.M. Zhilin, Y.A. Ossipyan,T. Bredow, and I. Mertig, J. Appl. Phys. **104**, 083704 (2008)

[83] Shun Yu, S. Ahmadi, C. Sun, P.T.Z Adibi, W. Chow, A. Pietzsch and M. Göthelid, J. Chem. Phys. **136**, 154703 (2012)

[84] P. Gargiani, M. Angelucci, C. Mariani, and M.G. Betti, Phys. Rev. B**81**, 085412 (2010)

[85] B. Brena, C. Puglia, M. de Simone, M. Coreno, K. Tarafder, V. Feyer, R. Banerjee, E. Göthelid, B. Sanyal, P.M. Oppeneer, and O. Eriksson, J Chem. Phys. **134**, 074312 (2011)

[86] M. -S. Liao, and S. Scheiner, J. Chem. Phys. **114**, 9780 (2001)

[87] W. Chen, C. Huang, X.Y. Gao, L. Wang, C.G. Zhen, D. Qi, S. Chen, H.L. Zhang, K.P. Loh, Z.K. Chen, A. Thye, and S. Wee, J. Phys. Chem. B **110**, 26075-26080 (2006)

[88] K. Walzer, B. Maeninh, M. Pfeiffer, and K. Leo, Chem. Rev. **107**, 1233-1271 (2007)

[89] H. Ding, K. Park, K. Green, and Y. Gao, Chem. Phys. Lett. **454**, 229-232 (2008)

[90] T. Schwieger, H. Peisert, M. S. Golden, M. Knupfer, and J. Fink, Phy. Rev. B **66**, 155207 (2002)

[91] Y. Bai, F. Buchner, M. Wendahl, I. Kellner, A. Bayer, H.-P., Steinrück, H. Marbach, J. Gottfried, J. Phys. Chem. C, **112**, 6087 (2008)

[92] L. Giovanelli, P. Vilmercati, C. Castellarin-Cudia, J.-M. Themlin, L. Porte, and A. Goldoni, J. Chem. Phys. **126**, 44709 (2007)

Acta Universitatis Upsaliensis

Digital Comprehensive Summaries of Uppsala Dissertations from the Faculty of Science and Technology 941

Editor: The Dean of the Faculty of Science and Technology

A doctoral dissertation from the Faculty of Science and Technology, Uppsala University, is usually a summary of a number of papers. A few copies of the complete dissertation are kept at major Swedish research libraries, while the summary alone is distributed internationally through the series Digital Comprehensive Summaries of Uppsala Dissertations from the Faculty of Science and Technology.

Distribution: publications.uu.se
urn:nbn:se:uu:diva-173505

ACTA
UNIVERSITATIS
UPSALIENSIS
UPPSALA
2012